Origin of volatiles emitted by Plinian mafic eruptions of the Chikurachki volcano, Kurile arc, Russia: trace element, boron and sulphur isotope constraints

Andrey A. Gurenko[a,b]*, Alexander B. Belousov[c], Vadim S. Kamenetsky[d,e], Michael E. Zelenski[e]

[a] *Woods Hole Oceanographic Institution, Woods Hole, MA 02543, USA*

[b] *Centre de Recherches Pétrographiques et Géochimiques, Université de Lorraine, 54501 Vandoeuvre-lès-Nancy, France*

[c] *Institute of Volcanology and Seismology, Petropavlovsk-Kamchatsky, 683006, Russia*

[d] *School of Physical Sciences, University of Tasmania, Hobart, TAS 7001, Australia*

[e] *Institute of Experimental Mineralogy RAS, Chernogolovka, 142432, Russia*

Revised manuscript

for submission to *Chemical Geology*

12 September, 2017

Components: abstract (398 words; 2,628 characters with spaces),

main text (9,672 words; 61,177 characters with spaces),

11 figures, 2 tables,

the list of references includes 178 citations.

*** Corresponding author and present address:** Andrey A. Gurenko, Centre de Recherches Pétrographiques et Géochimiques, 15, rue Notre-Dame des Pauvres, BP 20, 54501 Vandoeuvre-lès-Nancy, France. Phone: +33 (0)3 83 59 48 75, Fax: +33 (0)3 83 51 17 98, E-mail: agurenko@crpg.cnrs-nancy.fr

Abstract – Chikurachki is a 1816-m high stratovolcano on Paramushir Island, Kurile arc, Russia, which has repeatedly produced highly explosive eruptions of mafic composition. The present work is aimed at constraining the origin of volatile components (CO_2, H_2O, F, S, and Cl), along with B and S isotopic compositions in a series of phenocryst-hosted melt inclusions and groundmass glasses from basaltic andesite pyroclasts of the 1853, 1986, and prehistoric Plinian eruptions of the volcano. The ranges of volatile concentrations in melt inclusions (47–1580 μg/g CO_2, 0.4–4.2 wt.% H_2O, 399–633 μg/g F, 619–3402 μg/g S and 805–1240 μg/g Cl) imply a sudden pressure release from ~460 through ~35 MPa that corresponds to ~1.2–16-km-depth range of magma ascent upon decompression. We conclude that rapid ascent of the volatile-rich basaltic magmas from ~16-km initial depth accompanied by near-surface bubble nucleation and growth, and subsequent magma fragmentation appear to be a primary reason for the Plinian character of the Chikurachki eruptions. Significant negative correlations of S with K, Zr, Nb, Ba, La, Ce, Pr (R = –0.8 to –0.9), no clear relationships of S with H_2O, CO_2 and Cl, but strong positive correlations of S/K_2O with H_2O/K_2O, Cl/K_2O and F/K_2O preclude magma degassing to be the only process affecting volatile concentrations dissolved in the melt. The $\delta^{34}S$ values of the studied inclusion and groundmass glasses range from –1.6 to +12.3‰, decrease with decreasing S, show significant positive correlations with H_2O/K_2O, Cl/K_2O and F/Zr, and negative correlations with a number of incompatible trace elements. Neither open- nor close-system magma degassing can account for the observed range of $\delta^{34}S$. The $\delta^{11}B$ values of the melt inclusions range from –7.0 to +2.4‰ with 13–23 μg/g B. The relationships of $\delta^{11}B$ with B/K_2O and B/Nb are inconsistent with magma contamination at shallow crustal depths. Linear character of 1/S vs. $\delta^{34}S$ relationship suggests two-component mixing. The possible mixing end-members could be the magmas having similar major and trace element compositions, but strongly contrasting volatile contents and S isotopes. Based on the behaviour of fluid-mobile vs. fluid-immobile incompatible trace elements, we conclude that the subduction component likely

represents a mixture of subduction sediment-derived melt with up to 60% of slab-derived fluid. Admixture of ~1–8% of the inferred subduction component to the depleted mantle wedge source is required to account for the compositional range of the Chikurachki melt inclusions, and ~0.4–10% to account for the composition of Kurile arc mafic magmas.

Keywords

Plinian mafic eruptions, Chikurachki volcano, Melt inclusions, Magmatic volatiles, Stable isotopes, Ion microprobe

Research Highlights

- Origin of volatiles that caused Plinian basaltic eruptions of Chikurachki was studied.
- Degassing cannot account for the observed ~14‰ range of δ^{34}S in melt inclusions.
- Behaviour of volatiles and δ^{11}B in inclusion glasses precludes crustal contamination.
- Volatiles and δ^{34}S of the glasses were mainly controlled by two-component mixing.
- The subduction component was a 4:6-mixture of slab-derived melt and fluid.

1. Introduction

Strongly explosive (Plinian) eruptions are characterised by high eruption rates, high eruption columns and widely dispersed fallout deposits, representing an efficient mechanism to transport volatiles from the Earth's interior to the upper atmosphere (Walker, 1973, 1980; Fischer and Schmincke, 1984; Wilson and Walker, 1987; Francis, 1993). Injection of water, halogens and sulphur into the atmosphere leads to the formation of solid and liquid aerosols, which may significantly affect global climate and the stability of the ozone layer (Brasseur and Granier, 1992). Plinian eruptions are mainly associated with water-rich intermediate and silicic magmas (andesite through dacite), whereas highly explosive eruptions of mafic composition (i.e., resembling basalt or basaltic andesite) are less common. Examples of Plinian mafic eruptions occur at Klyuchevskoy, Tolbachik, Chikurachki and Tyatya in the Kamchatka and Kurile arcs, Russia (Fedotov and Markhinin, 1983; Ovsyannikov and Muravyev, 1992; Belousov et al., 2003, 2015, 2017; Hasegawa et al., 2011), Masaya and Cerro Negro, Nicaragua (Williams, 1983; Roggensack at al., 1997), Arenal, Costa Rica (Soto and Alvarado, 2006; Szramek et al., 2006), Llaima, Chile (Ruth et al., 2016), Sumisu Rift, Japan (Gill et al., 1990), Ambrym, Vanuatu (Robin et al., 1993), Tofua, Tonga (Caulfield et al., 2011), Taupo and Tarawera, New Zealand (Walker, 1980; Walker et al., 1994), Shishaldin, Alaska (Szramek et al., 2010) and Etna, Italy (Houghton et al., 2004; Sable et al., 2006). The lack of clear relationships between eruption rate and style often associating with rapid change of eruptive behaviour of a volcano suggest that many different parameters such as conduit geometry, magma viscosity, changing conditions of magma ascent and fragmentation, and even the dynamics of syn-eruptive microlite growth may strongly affect the eruption figure (e.g., Fischer and Schmincke, 1984; Carey and Sparks, 1986; Houghton et al., 2004; Szramek et al., 2006, 2010; Houghton and Gonnermann, 2008).

The present work is a follow-up study to Gurenko et al. (2005a) and focuses on the detailed investigation of the behaviour of volatile components (CO_2, H_2O, F, S, and Cl) along with boron and sulphur isotopic compositions of the previously analysed olivine-,

orthopyroxene- and plagioclase-hosted melt inclusions and groundmass glasses erupted by the Chikurachki volcano. Volatile-rich slab-derived melts and fluids play a central role in the origin of arc magmatism by lowering the solidus of a peridotite mantle wedge and triggering partial melting (e.g., Gill, 1981; McCulloch and Gamble, 1991; Hawkesworth et al., 1993; Pearce and Peate, 1995). Being a major inventory and a transport media of volatile components from descending plate to the overlying mantle, these melts and fluids (along with the factors listed above) may also have a link to the eruption style of volcanoes occurring in the subduction zone (SZ) setting. Here we explore the role of two concurrent processes, namely, subduction-related volatile flux versus possible gain of volatile components due to shallow crustal contamination of magma, also in relation of their possible contribution to the enrichment/depletion of the magma by sulphur and boron isotopes. Our new data provide additional constraints on the origin of volatile components in the mafic magmas erupted by the Chikurachki volcano during Plinian prehistoric and recent, 1853 and 1986 eruptions.

Another key problem in understanding the origin of arc magmas is the uncertainty in the provenance of volatile components. For example, Cl and H_2O are thought to be primarily (>95%) from the subducting slab (e.g., Straub and Layne, 2003), whereas S and F can originate from metasomatically enriched subarc mantle or come directly from the slab (e.g., Alt et al., 1993; Metrich et al., 1999; Straub and Layne, 2003; Churikova et al., 2007; Selvaraja et al., 2017). Moreover, with increasing of subduction depth, the slab becomes progressively depleted in H_2O and Cl, and to a lesser extent in S and F, implying efficient fractionation of H_2O and Cl from S and F (e.g., Chaussidon et al., 1987; Metrich et al., 1999; Straub and Layne, 2003). Understanding the origin of volatiles that triggers the Plinian eruption of Chikurachki may also contribute to our understanding of fluid dynamics and mass transport in SZ settings, as well as help in elucidating the relative contributions of different subduction components to the generation of arc magmas.

2. Geological setting and samples

Chikurachki (50°19′24″N 155°27′39″E, 1816 m.a.s.l) is an active stratovolcano on Paramushir Island, the northern Kuriles (**Fig. 1**). The volcanism of Chikurachki results from westward subduction of the Pacific plate under the Okhotsk plate. The Late Holocene stratocone of the volcano is built on a thick sequence of Pleistocene lava flows (Gorshkov, 1967). The recorded activity on Chikurachki started around 7500 BC. According to the Kamchatka Volcanic Eruption Response Team (KVERT), the most recent eruptions of 1958, 1961, 1964, 1973, 2002, 2003, 2004, 2005, 2007, 2008 were predominately of strombolian (mildly explosive), but recent Plinian (highly explosive) eruptions occurred in 1853, 1986 (**Fig. 2**), and the last one in 2015.

2.2. Samples studied

This study is based on the analyses of glassy lapilli with porphyritic texture, which came from the 1853 (sample CHK3/4), 1986 (sample CHK16) and two prehistoric (samples CHK13/1 and 13/2) tephra fallouts, resulting from documented, highly explosive eruptions of Chikurachki (Ovsyannikov and Muravyev, 1992; Belousov et al., 2003). We studied primary melt inclusions hosted by olivine, orthopyroxene and plagioclase phenocrysts, most of which were naturally quenched to glass. Chemical compositions of the studied inclusions and groundmass glasses (major and trace element, and H_2O, S and Cl concentrations) were reported by Gurenko et al. (2005a). Briefly, the erupted melts range from low- to medium-K tholeiitic basalts and andesites, which are typical for Kurile lavas (**Fig. S2.1** – *Supporting online material*). Variation diagrams of FeO, CaO and K_2O vs. SiO_2 show that glass compositions follow simple trends of magma fractionation (Fig. 5 in Gurenko et al., 2005a). The phenocrysts are dominated by euhedral, elongated, twinned individual crystals of plagioclase (Pl, ~0.2–3.0 mm, 70–90 vol.%, $An_{74–95}$) that may also form glomerocrysts. Phenocrysts of subhedral to rounded olivine (Ol, $Fo_{72–78}$) and orthopyroxene (Opx, *mg*-number = 72–75), both of 0.2–0.5 mm size, and euhedral to resorbed

clinopyroxene (Cpx, 0.3–1.0 mm, *mg*-number = 71–77) are present in subordinate amounts. The groundmass is strongly vesiculated (20–30 vol.% vesicles) and consists of variable proportions of rounded olivine, prismatic augite and isometric Fe-Ti oxide crystals mixed with needle-like plagioclase microlites (up to 200 µm).

The studied inclusion and groundmass glasses are slightly enriched in light rare earth elements (LREE) relative to heavy rare earth elements (HREE); e.g., $[La/Sm]_n$ = 1.8–2.4, where the subscript *n* denotes the respective element concentrations normalised to those of N-MORB taken from Hofmann (1988) (**Fig. 3, Table S2.1** – *Supporting online material*). The glasses also show significant depletions in high-field-strength elements (HFSE) relative to LREE but nearly equal concentrations of HFSE relative to HREE normalised to N-MORB (e.g., $[Nb/La]_n$ = 0.19–0.29, $[Zr/Sm]_n$ = 0.52–0.76, $[Y/Yb]_n$ = 0.86–1.24), and enrichments in Th and large-ion lithophile elements (LILE) relative to Nb (e.g., $[Ba/Nb]_n$ = 41–69, $[Th/Nb]_n$ = 7–30, $[K/Nb]_n$ = 15–25 and $[Sr/Sm]_n$ = 2.9–6.9). The inclusions, and to lesser extent the groundmass glasses are characterised by relatively high contents of volatile components (the concentrations of B, H_2O, Cl and F shown in **Fig. 3** are discussed in section 4.1), displaying positive anomalies in the multi-element diagram relative to respective trace elements of similar incompatibility (e.g., $[Cl/Nb]_n$ = 21–54, $[B/K]_n$ = 2.3–5.4, $[H_2O/Ce]_n$ = 4.9–23, $[F/Nd]_n$ = 2.2–3.2, $[F/Zr]_n$ = 3.9–7.8). These values are generally in, or slightly exceeding, the range of volatile concentrations reported for the Kurile island arc basalts and basaltic andesites (MgO >2.5 wt.%) by Bailey et al. (1987a,b), Ishikawa and Tera (1997), Ikeda (1998), Ikeda et al. (2000), Takagi et al. (1999), Ishikawa et al. (2001) (**Fig. 3**).

3. Analytical methods

Ion microprobe analyses were obtained with a CAMECA IMS 1280 ion microprobe at the Northeast National Ion Microprobe Facility (Woods Hole Oceanographic Institution, Woods

Hole, USA) (for detailed description of the employed analytical protocols, see *Supporting online material*).

4. Results

4.1. Volatile concentrations

The concentrations of CO_2, H_2O, F, S, and Cl in naturally quenched, glassy inclusions hosted in Ol, Opx and Pl are listed in **Table S2.1** *(Supporting online material)*, along with H_2O, S and Cl reported by Gurenko et al. (2005a). The inclusions have a wide range of volatile concentrations (39–653 μg/g CO_2, 0.4–4.2 wt.% H_2O, 428–638 μg/g F, 676–3450 μg/g S, and 805–1243 μg/g Cl) that corresponds to the volatile contents previously reported by Gurenko et al. (2005a). Correction for post-entrapment crystallisation (PEC) of host mineral (up to 7.8 wt.% Ol, 0.8 wt.% Opx, and no correction for Pl) results in the following ranges: 39–626 μg/g CO_2, 0.4–4.2 wt.% H_2O, 412–634 μg/g F, 639–3408 μg/g S, 805–1241 μg/g Cl, which appeared to be nearly the same (given the maintained analytical uncertainty) as the uncorrected volatile concentrations. This observation implies that the eruption and quenching of magma occurred shortly after the inclusions have been entrapped by growing phenocrysts. Thus, the concentrations of H_2O and CO_2 measured in the studied melt inclusions reflect the last vapour-melt equilibrium in the magmatic system upon the eruption, returning a minimum pressure of magma fractionation. According to the *VolatileCalc* solution model (Newman and Lowenstern, 2002), they correspond to H_2O-CO_2 gas pressure of 33 to 276 MPa or to the range of depth from ~1 to ~9.5 km, assuming average and constant density of ~2900 kg/m^3 of the upper crust **(Fig. 4A)**.

Several recent studies (Esposito et al., 2011; Steele-Macinnis et al., 2011; Hartley et al., 2014; Moore et al., 2015; Wallace et al., 2015; Mironov et al., 2015; Aster et al., 2016) have demonstrated that 40 to 90% of the original CO_2 dissolved in the melt at the time of inclusion

197 entrapment can be lost to a shrinkage bubble during post-entrapment cooling. A correction
198 algorithm described by Wallace et al. (2015) was therefore used to reconstruct the original CO_2
199 and H_2O concentrations in the entrapped melts (see *Supporting online material*). These
200 calculations revealed that ~5 to 69% of the original CO_2 and 0.1 to 3.2% of the original H_2O
201 could have been lost to the shrinkage bubble, in agreement with the results of the above studies.
202 The following ranges of volatile concentrations were obtained after the correction: 47–1580 µg/g
203 CO_2, 0.4–4.2 wt.% H_2O, 399–633 µg/g F, 619–3402 µg/g S and 805–1240 µg/g Cl (**Table S2.1**
204 – *Supporting online material*). According to the *VolatileCalc* solution model (Newman and
205 Lowenstern, 2002), the corrected results correspond to the H_2O-CO_2 gas pressures between 35
206 and 456 MPa or to ~ 1.2–15.7-km-range of crustal depth **(Fig. 4B)**.
207 The concentrations of S in melt inclusions are shown in comparison with mid-ocean ridge
208 basalts (MORB) and ocean island basalts (OIB) (**Fig. 5A**). Many of the Chirurachki glass
209 inclusions have similar or higher S concentrations than those of MORB or OIB, whereas all
210 groundmass glasses are depleted in S (<350 µg/g), consistent with sulphur loss presumably by
211 degassing. However, sulphur in the inclusion glasses shows significant negative correlations with
212 a number of trace and rare earth incompatible elements, such as K (–0.81), Ti (–0.59), Y (–0.61),
213 Zr (–0.82), Nb(–0.71), Ba (–0.83), La (–0.79), Ce (–0.88), Pr (–0.77), Nd (–0.71), Sm (–0.68),
214 Gd (–0.56), Dy (–0.73), Ho (–0.53), Er (–0.73), Yb (–0.66), Lu (–0.71), Th (–0.66), where the
215 respective correlation coefficient (R) values are given in brackets and N = 21, if not specified
216 (**Fig. 5B** and **Table S2.1** – *Supporting online material*). All these correlations are significant at
217 95% confidence level (for N = 18 and 21, a number of points in the correlations, a critical value
218 of the Pearson correlation coefficient at the 0.05-level of significance for a two-tailed test is 0.47
219 and 0.43, respectively). There are no significant correlations of S with H_2O, Cl and F. We
220 observe, however, strong positive correlation between these elements, if their concentrations are
221 normalised to K_2O (or any other melt- and fluid-immobile incompatible element) that minimises

possible effects of partial melting and/or magma fractionation (e.g., R = 0.83 for S/K_2O vs. H_2O/K_2O correlation, **Fig. 5C**, R = 0.80 for S/K_2O vs. Cl/K_2O, **Fig. S2.1A** – *Supporting online material*, R = 0.85 for S/K_2O vs. F/K_2O, **Fig. 5D**, and R = 0.88 for Cl/K_2O vs. H_2O/K_2O, **Fig. 5E**). Chlorine does not correlate with incompatible trace elements, except for Sr (R = –0.56; **Fig. S2.1B** – *Supporting online material*), shows a significant correlation with fluorine (R = 0.70; **Fig. S2.1C** – *Supporting online material*), which becomes much stronger, if we consider F/Zr vs. Cl/Nb ratios (R = 0.88; **Fig. 5F**).

4.2. Sulphur isotopes

Sulphur isotopic compositions of the studied melt inclusions and one groundmass glass are given in **Table S2.1** *(Supporting online material)* and presented in **Fig. 6**. The $\delta^{34}S$ values are given in permil units (‰) relative V-CDT (the Vienna Canyon Diabolo Troilite, $^{34}S/^{32}S$ = 0.0441626 ± 0.0000039; Ding et al., 2001). The $\delta^{34}S$ values of the inclusion glasses range from –1.6 to +12.3‰, and decrease with decreasing S concentrations (R = 0.85; **Fig. 6A**). The S vs. $\delta^{34}S$ relationship has a hyperbolic shape and is transformable into a strait line in the 1/S-$\delta^{34}S$ space (R = –0.84; **Fig. 6B**), pointing towards two-component mixing scenario (Langmuir et al., 1978), though the effect of magma degassing cannot be completely excluded (see further discussion). The sample 13/1 matrix glass has $\delta^{34}S$ = +0.39 ± 0.43‰, 1 SE, contains very low S concentration (107 µg/g S) and strongly deviates from the linear array defined by melt inclusions (**Fig. 6B**), being in contrast strongly degassed. Also, the $\delta^{34}S$ values show significant positive correlations with H_2O (0.54), CO_2 (0.55) and Sr (0.5), as well as negative correlations with light lithophile elements Li (–0.53, N = 10), Be (–0.73, N = 10) and B (–0.6), and other incompatible elements, such as K (–0.8), Zr (–0.71), Nb (–0.64), Ba (–0.75), La (–0.69), Ce (–0.72), Pr (–0.57), Sm (–0.63), Gd (–0.76), Dy (–0.71), Tb (–0.49), Er (–0.8), Lu (–0.79), Th (–0.53), where the respective correlation coefficient (R) values are given in brackets and N = 17, if not

247 specified, and the critical value of the Pearson correlation coefficient is 0.48. The significance of
248 the correlations of δ^{34}S with volatile components becomes higher, if volatile concentrations are
249 normalised to incompatible elements as, for instance, H_2O/K_2O (0.79), Cl/K_2O (0.83) (**Fig.**
250 **6B,C**), F/Zr (0.84, **Fig. S2.1D** – *Supporting online material*).
251
252 *4.3. Boron concentrations and B isotopic composition*
253 The concentrations of boron (12.5–22.9 μg/g measured, and 12.5–21.7 μg/g corrected for
254 PEC) are similar to those previously reported by Gurenko et al. (2005a) (16.1–18.7 μg/g B)
255 (**Table S2.1** – *Supporting online material*). The B/K ratios ranging from 0.0025 to 0.0057 are
256 systematically higher than those of primitive N-MORB (B/K of ~0.001) and OIB (B/K of
257 ~0.0003) (Ryan and Langmuir, 1993; Chaussidon and Jambon, 1994; Gurenko and Chaussidon,
258 1997) but are in the midrange of B concentrations reported for Kurile arc magmas with SiO_2 <60
259 wt.% (4.5–36.6 μg/g B; Ryan et al., 1995; Ishikawa and Tera, 1997). Very similar concentrations
260 of B in the Chikurachki lavas (14.4–15.5 μg/g) were found, in particular, by Ishikawa and Tera
261 (1997), who also noted a clear across-arc variation of B/Nb ratios (and δ^{11}B, as well). At the slab
262 depth of ~140 km corresponding to that of the Chikurachki volcano (e.g., Tatsumi et al., 1994;
263 Ishikawa and Tera, 1997; Ishikawa et al., 2001 and references therein), the B/Nb ratios in the
264 Kurile lavas vary from ~6 to 18 (Ishikawa and Tera, 1997), and the present B/Nb range obtained
265 for the studied melt inclusions (from ~9 to ~22) is in agreement with these data.
266 The δ^{11}B values of the studied naturally quenched olivine-hosted melt inclusions range
267 from –7.0 to +2.4‰, calculated relative to NBS 951 standard with $^{11}B/^{10}B = 4.04558 \pm 0.00033$
268 (Spivack and Edmond, 1986) (**Table S2.1** – *Supporting online material*). The range is similar but
269 extends to more negative values than those of the Kurile arc lavas (from –3.8 to +5.9‰;
270 Ishikawa and Tera, 1997), being however within a broad interval of δ^{11}B-values of arc magmas
271 worldwide, from –21.3‰ (e.g., Mt. Shasta; Rose et al., 2001) to +12‰ (e.g., Izu arc; Straub and

Layne, 2002). In contrast to S isotopes, δ^{11}B values show neither a correlation with the concentrations of B or 1/B values nor with major and incompatible trace elements. Similarly, a wide δ^{11}B range of ~20‰ (from −21.3 to −1.1‰ at relatively narrow range of boron concentrations (0.67–1.64 μg/g B) showing no clear correlation between each other was described in the Mt. Shasta basaltic andesite rocks (Rose et al., 2001).

5. Discussion

5.1. H_2O-Cl-B and δ^{11}B relationships and the magma contamination scenario

Assimilation of crustal rocks is a common process that can significantly modify pristine chemical and isotopic compositions of parental arc magmas (e.g., Davidson, 1987; Thirlwall et al., 1996; Hickey et al., 1986; Turner et al., 1997; Macpherson and Mattey, 1998; Vroon et al., 2001; Bindeman et al., 2004; Walowski et al., 2016). Excess of halogens in mafic magmas, and especially coherent variation of H_2O and Cl was shown to be a good proxy to assess the role of assimilation of oceanic crust and/or addition of NaCl-rich brines or fluids during magma fractionation (e.g., Anderson, 1974; Michael and Schilling, 1989; Jambon et al., 1995; Michael and Cornell, 1998; Kent et al., 1999; Lassiter et al., 2002; Simons et al., 2002; le Roux et al., 2006; Shimizu et al., 2009; Gurenko and Kamenetsky, 2011; Kendrick et al., 2013, Cabral et al., 2014). However, as noted by le Roux et al. (2006), this approach is based on the assumption that the concentration of K_2O in the magma remains unaffected by later processes. These authors recommend using Cl/Nb and H_2O/Ce ratios because Nb and Ce have similar incompatible behaviour to Cl and H_2O, respectively, but are less affected by alteration, as compared to K.

In our case, a positive correlation of H_2O/K_2O with Cl/K_2O in the Chikurachki melt inclusions (**Fig. 5E**) can be interpreted in favour of magma contamination. However, strong positive correlations between H_2O/K_2O and H_2O/Ce (R = 0.97, not shown) and between Cl/K_2O and Cl/Nb (R = 0.88, not shown) suggest that K, Nb and Ce appear to behave coherently during

297 magma fractionation. Furthermore, the concentrations of K are unlikely to have been
298 compromised and could be equally used for normalisation. The results of concurrent modelling
299 of magma contamination using different compositions of probable crustal contaminants are
300 shown in **Fig. 7** and **8**. In the modelling, we use the same element concentrations and δ^{11}B values
301 of seawater (SW), 15%- and 50%-NaCl brine (15%-NaCl and 50%-NaCl, respectively), and
302 altered oceanic crust (AOC) mixing end-members, as in Gurenko and Kamenetsky (2011)
303 (**Table 1**). Given the narrow range of incompatible element concentrations in the studied melt
304 inclusions (**Fig. 3**), the concentrations of K_2O (0.804 wt.%), Nb (1.28 μg/g) and Ce (15.37 μg/g)
305 of a presumably "uncontaminated" arc magma (UAM) were defined as average of all melt
306 inclusions from **Table S2.1** – *Supporting online material* (using PEC-corrected concentrations).
307 The boron content and B isotopic composition of UAM (0.9 μg/g B, δ^{11}B = –3.7‰)
308 corresponding to back-arc basin basalts presumably unaffected by later shallow-crustal
309 contamination were taken from Chaussidon and Marty (1995). The concentrations of H_2O and Cl
310 in UAM were calculated using those of the neighbouring elements of similar incompatibility but
311 showing no anomalies in the multi-element diagram (**Fig. 3**) to be in the lower left corner of the
312 respective panels in **Fig. 7**, thereby matching the lower end of the trends defined by the inclusion
313 compositions: $[H_2O]_n = ([Ce]_n \times [Pr]_n)^{0.5}$, equal to 0.256 wt.% H_2O, and $[Cl]_n = ([Nb]_n \times [K]_n)^{0.5}$,
314 equal to 128.5 μg/g Cl. The chemical and isotopic compositions of seawater (SW) is relatively
315 uniform and well constrained, whereas the composition of seawater-derived NaCl-brines can be
316 calculated from that of SW (**Table 1**). In contrast, the composition of altered oceanic crust
317 (AOC) is variable. In particular, AOC from Gurenko and Kamenetsky (2011) is significantly
318 more H_2O-, Cl- and K_2O-rich than that used for similar calculations by le Roux et al. (2006). In
319 order to account for possibly wider ranges of H_2O, Cl, Nb and Ce, we considered two
320 compositions of AOC: AOC1 from Gurenko and Kamenetsky (2011) and AOC2 from le Roux et
321 al. (2006) (**Table 1**). Finally, we assigned a composition of siliceous marine sediment (SED),

322 which is considered as one possible, if not a single contamination component to account for the
323 negative δ^{11}B melt inclusion values, with 10.1 wt.% H_2O, 1.7 wt.% K_2O, 7.67 μg/g Nb, 50.11
324 μg/g Ce. The concentrations of H_2O, K_2O, Nb and Ca used in calculations are those of the
325 average sediment column of the Kurile trench from Plank and Langmuir (1998), and 1000 μg/g
326 Cl, 120 μg/g B, and δ^{11}B = −10‰ were taken from Gurenko and Kamenetsky (2011), given that
327 siliceous terrigenous sediments may be as low as −15‰ of δ^{11}B (Leeman and Sisson, 1996).

328 As noted by Gurenko and Kamenetsky (2011), it is not possible to unequivocally prove
329 magma contamination only on the basis of H_2O/K_2O vs. Cl/K_2O relationships (or using Cl- and
330 H_2O-to-incompatible-element normalised ratios). Similarly, if we consider solely the H_2O/K_2O
331 vs. Cl/K_2O or H_2O/K_2O-B/K_2O variations in melt inclusions (equally, H_2O/Ce vs. Cl/Nb or
332 H_2O/Ce vs. B/Nb), they can be explained by contamination of magma by seawater or NaCl-rich
333 brines (**Fig. 7**). On the other hand, if in addition to H_2O and Cl we consider boron content and B-
334 isotope data then the relationships between Cl/K_2O and B/K_2O (equally, Cl/Nb vs. B/Nb; **Fig.**
335 **S2.2C** – *Supplementary online material*), or B/K_2O (or B/Nb) vs. δ^{11}B (**Fig. 8**) confirm neither
336 significant contribution of these components, nor the contribution of AOC1, AOC2 and SED
337 components. Indeed, to account for the compositions of melt inclusions with strongly and
338 coherently varying H_2O/K_2O = 0.3–8.9 and Cl/K_2O = 0.06–0.24, it would require contamination
339 either by SW (up to 7%) or more concentrated NaCl-brine, or assimilation of AOC1 (up to 60%)
340 or both AOC1 + SW components (**Fig. 7A**). No significant effect of 15%-NaCl and 50%-NaCl
341 brine, as well as the role of AOC2 and SED can be recognised in this diagram. The same
342 conclusions can be derived from the H_2O/Ce vs. Cl/Nb variations (**Fig. 7B**), with only a
343 difference that contamination by AOC1 (up to 70%) is required. However, if we consider mixing
344 of the same components in coordinates H_2O/K_2O vs. B/K_2O or H_2O/Ce vs. B/Nb (**Fig. 7C,D**),
345 then the role of SW and AOC1, along with 15%-NaCl and AOC2 is not yet justified, but the
346 50%-NaCl end-member appears to be potentially significant. The amount of SED to add to UAM

appears to be up to 50% in **Fig. 7C** and up to 100% in **Fig. 7D**, both being unrealistic. Finally, if we consider B/K_2O vs. $\delta^{11}B$ or B/Nb vs. $\delta^{11}B$ systematics (**Fig. 8**), then the role of seawater, NaCl-brines and AOC1 is not confirmed at all, while the amount of AOC2 and SED to be assimilated approaches to 100% (**Fig. 8B**).

In conclusion we note that Cl and F often behave as incompatible elements during partial melting and magma fractionation (e.g., Fischer and Schmincke, 1984; Carroll and Webster, 1994; Jambon, 1994; Dalou et al., 2014). As shown by Dalou et al. (2014 and references therein), a Cl/F ratio of >1 is expected in arc magmas resulting from partial melting of a depleted mantle source mixed with an aqueous dehydration fluid because the Cl/F ratio in the subduction slab fluids is usually high (e.g., ~4 in Mount Shasta rocks and up to 9.5 in Izu Bonin arc magmas). In contrast, the low Cl/F ratios (<1; e.g., Central and South American arcs, Kermadec) suggest that the magmas were produced by melting of a mantle source mixed with a hydrous slab melt. In this context, it is essential to note that Cl/F ratios in the studied melt inclusions range from 1.5 to 2.0, pointing towards predominant role of the subduction slab fluid in the origin of Chickuracki magmas. Finally, the observed relationships of S/K_2O with K_2O-normalised concentrations of H_2O, Cl and F (**Fig. 5C,D** and **Fig. 2.1A** – *Supporting online material*), as well as the H_2O/K_2O vs. Cl/K_2O and F/Zr vs. Cl/Nb correlations (**Fig. 5E,F**) strongly suggest that the variations of H_2O, S, Cl and F contents were not primarily affected by degassing or contamination, but more likely related to the transport of these components to magma source region by subduction slab fluids, in agreement with the previous studies of the Kurile-Kamchatka arc volcanism (e.g., Hochstaedter et al., 1996; Ishikawa and Tera, 1997; Kepezhinskas et al., 1997; Dorendorf et al., 2000; Churikova et al., 2001, 2007; Ishikawa et al., 2001; Portnyagin et al., 2007, 2015, Konrad-Schmolke et al., 2016).

5.2. Origin of sulphur concentration and S-isotope ranges

Sulphur solubility in basaltic magmas was shown to be mostly a function of iron content of the melt, if sulphur is predominately present in sulphide (S^{2-}) form (e.g., Connolly and Haughton, 1972; Haughton et al., 1974; Mathez, 1976; Carroll and Rutherford, 1985; Wallace and Carmichael, 1992;), but it also depends strongly on temperature, pressure, redox conditions, H_2O content, and the composition of coexisting melt and vapour phase (Nagashima and Katsura, 1973; Katsura and Nagashima, 1974; Carroll and Rutherford, 1985, 1987; Luhr, 1990; Wallace and Carmichael, 1992; Mavrogenes and O'Neill, 1999; Matjuschkin et al., 2016; Canil and Fellows, 2017; Mavrogenes and Blundy, 2017). The solubility of sulphur is generally higher (at a given f_{O_2}) in mafic (tholeiite and hawaiite), as compared to more SiO_2-rich magmas (rhyodacite) (e.g., Katsura and Nagashima, 1974).

As a sulphide-saturated melt becomes progressively oxidised, higher amount of sulphur is required to be dissolved in the melt to cause saturation of the melt with sulphide (e.g., Carroll and Webster, 1994 and references therein). This is also evident from the exponential character of FeO-S relationships observed in the more S-rich inclusions (**Fig. 5A**). The sulphur valence state changes from S^{2-} to S^{6+} within a limited range of oxygen fugacity, from NNO−1 to NNO+2 (Carroll and Rutherford, 1988; Wallace and Carmichael, 1994; Metrich and Clocchiatti, 1996; Gurenko and Schmincke, 2000; Jugo et al., 2005a,b, 2010; Fiege et al., 2015). Further melt oxidation causes a sulphide phase to become unstable. At these and more oxidised conditions (i.e., f_{O_2} is greater than NNO+2), anhydrite ($CaSO_4$) may become stable and appear as phenocrysts in the magma, as it was observed, for example, in some El Chichón and Mount Pinatubo trachyandesite and dacite magmas (Luhr et al., 1984; Varekamp et al., 1984; Carroll and Rutherford, 1987; Luhr, 1990; Bernard et al., 1991; Kress, 1997). Moreover, the solubility of sulphate (SO_4^{2-}) is much higher than that of sulphide (S^{2-}) in mafic magmas and can reach up to 2.5 wt.% SO_3 (Carroll and Rutherford, 1985, 1987; Luhr, 1990; Metrich and Clocchiatti, 1996; Gurenko and Schmincke, 2000; Jugo et al., 2005a,b; Fiege et al., 2015). Since S concentrations

in many of our inclusion glasses significantly exceed the level of S^{2-} solubility, and they show no correlation with FeO (**Fig. 5A**), we contend that a significant proportion of sulphur is dissolved as SO_4^{2-} species. This is consistent with generally higher oxidation state of subduction-zone-related magmas, and also with previously estimated oxygen redox conditions of the Chikurachki magmas (i.e., ΔNNO = +1 to +2; Gurenko et al., 2005a). According to the relationship given in Wallace and Carmichael (1994):

$$\log (X_{SO_4^{2-}}/X_{S^{2-}}) = a \log fO_2 + b/T + c \quad (1)$$

where $X_{SO_4^{2-}}$ and $X_{S^{2-}}$ are mole fractions of SO_4^{2-} and S^{2-} sulphur species in the melt (i.e., $X_{SO_4^{2-}} + X_{S^{2-}} = 1$), T is temperature in Kelvin, and coefficients a = 1.02, b = 25410, and c = –10, between 80 and 98% sulphur dissolved as SO_4^{2-} is expected in the basaltic melts representing the studied Plinian 1986, 1853 and prehistoric eruptions of the Chikurachki volcano, thereby explaining the elevated concentrations of sulphur in the studied melt inclusions.

The fact that sulphur isotopic composition (i.e., $\delta^{34}S$) strongly correlates with S concentrations in the melt inclusions and groundmass glasses (**Fig. 6A,B**), as well as with K_2O-normalised concentrations of H_2O and Cl (**Fig. 6C,D**) suggests that sulphur was more likely introduced to the magma by the same process along with H_2O and Cl. One possible and relatively simple explanation would be a contamination of magma by sulphate-bearing seawater-derived material at shallow-crustal depth, as it was previously demonstrated on example of Miocene basaltic hyaloclastites drilled during the ODP Leg 157 southwest of Gran Canaria (Canary Islands, Spain) by Gurenko et al., 2001. However, as discussed above, shallow-depth contamination was not a factor controlling budget of volatile components in the studied Chikurachki magmas. Thus, the origin of sulphur and its S-isotope signature could more likely

be ascribed to slab-derived fluids. Whether a consequent degassing of the magmas could result in the observed, nearly 14‰-range of $\delta^{34}S$ values is a subject of further discussion.

5.2.1. S-isotope fractionation during magma degassing

Magma degassing is an alternative process, which is capable to significantly affect the concentration and isotopic composition of sulphur in the melt by changing the proportion of the reduced (S^{2-}) and oxidised (SO_4^{2-}) forms (e.g., Taylor, 1986; Marini et al., 2011; Mandeville et al., 2009 and references therein). This is mostly because sulphide and sulphate species may possess strongly contrasting $\delta^{34}S$ values, with an average fractionation factor of +7.3 ± 1.4‰ between sulphate and sulphide (e.g., Sakai et al., 1982, 1984). According to Holloway and Blank (1994), the variations of $\delta^{34}S$ values resulted from continuous volatile exsolution can be modelled either as closed-system (Eq. 2) or as open-system (i.e., Rayleigh distillation) degassing (Eq. 3):

$$\delta^{34}S_f = \delta^{34}S_i + 1000\,(1 - F)\ln \alpha_{gas-melt} \quad (2)$$

$$\delta^{34}S_f = (\delta^{34}S_i + 1000)\,(F^{\alpha_{gas-melt} - 1}) - 1000 \quad (3)$$

where subscripts *f* and *i* refer to the final and initial isotopic compositions of S in the melt, respectively, *F* is a fraction of sulphur remaining in the melt upon degassing, and $\alpha_{gas-melt}$ is a gas-melt S-isotope fractionation factor defined as:

$$\alpha_{gas-melt} = (^{34}S/^{32}S)_{gas}/(^{34}S/^{32}S)_{melt} \quad (4)$$

To calculate the parameter F in Eq. 2 and 3, we used S-concentrations in final ($[S]_f$) and initial ($[S]_i$) melts normalised to a concentration of an incompatible trace element (metal; $[Me]_f$ and $[Me]_i$, respectively) by the following equation:

$$F = ([S]_f \times [Me]_i) / ([S]_i \times [Me]_f) \quad (5)$$

using, in particular, the concentrations of Ce and K in the respective melts, and then the average was used. Two melt inclusions with the highest S concentrations and $\delta^{34}S$ values (*3/4-4-1* and *13/2-1*-2, PEC- and exsolution-corrected values; **Table S2.1** – *Supporting online material*) were taken to calculate the initial melt composition ($[S]_i$ = 3287 μg/g, $[Ce]_i$ = 9.54 μg/g, $[K]_i$ = 3592 μg/g, and $\delta^{34}S_i$ = +11.2‰).

Modelling of S isotopic fractionation caused by degassing is rather complicated because $\alpha_{gas-melt}$ can be either higher or lower than unity because it depends strongly on T, f_{O_2} and the proportion of SO_4^{2+} and S^{2-} species dissolved in the melt. Generally, a fractionation factor of ^{32}S and ^{34}S isotopes between gas phase and silicate melt ($\Delta^{34}S_{gas-melt}$) can be expressed as following (e.g., Sakai et al., 1982), assuming that isotopic equilibrium is maintained among all sulphur species in the gaseous and melt phases:

$$\Delta^{34}S_{gas-melt} = \delta^{34}S_{gas} - \delta^{34}S_{melt} \approx 1000 \ln \alpha_{gas-melt} =$$
$$= [X\delta^{34}S_{SO_2} + (1 - X)\delta^{34}S_{H_2S}] - [Y\delta^{34}S_{sulfide} + (1 - Y)\delta^{34}S_{sulfate}], \quad (6)$$

where X is the mole fraction of SO_2 in the SO_2-H_2S gas phase (i.e., $X_{SO_2} + X_{H_2S} = 1$), and Y is the mole fraction of sulphur dissolved in the melt as sulphide, and $1 - Y$ mole fraction of sulphur dissolved as sulphate. After multiplying and collecting terms, Eq. 6 can be expressed as:

$$1000 \ln \alpha_{gas-melt} = X\ 1000 \ln \alpha_{SO_2-H_2S} + Y\ 1000 \ln \alpha_{sulphate-sulphide} - \quad (7)$$
$$- 1000 \ln \alpha_{sulphate-H_2S}$$

The temperature dependences of the fractionation factors in Eq. 7 can be approximated by the relationships studied by Richet et al. (1977) and Miyoshi et al. (1984) (for more detail see a compilation by Taylor, 1986):

$$1000 \ln \alpha_{SO_2-H_2S} = -0.42 \times 10^9/T^3 + 4.367 \times 10^6/T^2 - 0.105 \times 10^3/T - 0.41 \quad (8)$$

$$1000 \ln \alpha_{sulphate-sulphide} = 7.4 \times 10^6/T^2 - 0.19 \quad (9)$$

$$1000 \ln \alpha_{sulphate-H_2S} = 6.5 \times 10^6/T^2 \quad (10)$$

where T is temperature in Kelvin. For the temperature range from 910 to 1180°C determined for the studied Chikurachki melt inclusions (Gurenko et al., 2005a), the $\Delta^{34}S_{gas-melt}$ fractionation factor is within the range of –2.1‰ to –0.9‰ (i.e., $\alpha_{gas-melt}$ = 0.9979–0.9991). The calculations were done assuming X = 0.98 because usually the volcanic gases emitted at temperatures ~1000°C contain mostly SO_2, whereas H_2S is present only in trace amount, as shown for Kilauea volcano, Hawaii, and Mnt. Etna, Sicily (Symonds et al., 1994) and according to the recent gas-melt equilibria model of Burgisser and Scaillet (2007) for oxidised (i.e., ΔNNO = +1.5) conditions. The variations of X within ±10% (from 0.8 to 1) will cause an uncertainty in the resulting $\Delta^{34}S_{gas-melt} \approx \pm 0.2–0.3$‰. The Y value varied from 0.02 to 0.2, in agreement with the previously reported ΔNNO-range from +1 to +2, resulting in 80 to 98% sulphur dissolved as sulphate in the melt (see above).

The diagram of $\delta^{34}S$ versus F (**Fig. 9**) demonstrates that neither open- nor close-system degassing can account for the observed ~14‰ range in the Chikurachki melt inclusions. This is mostly because the outgassed SO_2 will preferentially drive out the lighter ^{32}S isotope under

conditions of high f_{O_2} so that the remaining melt will be progressively enriched in ^{34}S, as it was first shown by Sakai et al. (1982) and also demonstrated by Mandeville et al. (2009) for the case of climatic and pre-climatic eruptions of Mt. Mazama, Crater Lake, Oregon, but being completely opposite to what is observed in **Fig. 6A** and **Fig. 9**. Negative correlations of S with incompatible trace elements mentioned above (**Fig. 5B**) may suggest that magma fractionation (resulting in enrichment of melt by incompatible trace elements) might have been accompanied by S-depletion due to degassing. However, a weak correlation of S with CO_2 and no correlations with other volatile components (like H_2O and Cl) imply that degassing, though being probably important, was not a single process affecting the concentrations of the dissolved S. Furthermore, the fact that the hyperbola-shaped relationship of $\delta^{34}S$ vs. S concentrations (**Fig. 6A**) is transformable into a strait line in the 1/S-$\delta^{34}S$ space (**Fig. 6B**) represents a strong argument in favour of two-component mixing hypothesis (Langmuir et al., 1978), whereas host lapilli groundmass glasses, which presumably suffered degassing, do not fit the line. We thus contend that sulphur abundances, the entire S-isotope range, as well as the other volatile components such as H_2O, Cl and F correlating with each other (**Fig. 5**) were largely controlled by two-component mixing process. The possible mixing end-members could be the magmas having similar major and trace element compositions but strongly contrasting volatile contents and S isotopes.

5.3. Trace element constraints on magma source components

Mafic arc magmatism results from melting of a mantle wedge, whose solidus is lowered by input of slab-derived hydrous melts and/or fluids (e.g., Gill, 1981; McCulloch and Gamble, 1991; Hawkesworth et al., 1993; Woodhead et al., 1993; Pearce and Peate, 1995). The composition of mantle wedge is relatively well constrained and thought to be represented by a MORB-type, or even more depleted upper mantle material (e.g., Woodhead et al., 1993;

519 Kepezhinskas et al., 1997). However, a relative contribution of slab-derived H_2O-rich fluids
520 and/or melts, as well as the proportion of the sediments relative to the mafic part of the oceanic
521 crust in the slab remains enigmatic. Numerous previous studies attempted to assess the effect of
522 fluid transport vs. slab melting in the origin of the Kurile-Kamchatka arc magmas (e.g.,
523 Hochstaedter et al., 1996; Ishikawa and Tera, 1997; Kepezhinskas et al., 1997; Khubunaya and
524 Sobolev, 1998; Dorendorf et al., 2000; Churikova et al., 2001, 2007; Ishikawa et al., 2001;
525 Portnyagin et al., 2007, 2015, Konrad-Schmolke et al., 2016, among others). One of the main
526 purposes of the present study is to constrain a contribution of the above mentioned components
527 to the origin of the Chikurachki magmas using the behaviour of fluid-immobile (i.e., Nb, Zr, Ti,
528 Yb) vs. fluid-mobile (i.e., B, Ba, K, Sr, ±Th) elements.
529
530 *5.3.1. Mantle wedge composition*
531 In our model calculations, it is essential to assess chemical composition of the mantle
532 wedge. Generally, the HFSE and HREE are immobile in the fluid and not enriched in the oceanic
533 crust and in sedimentary components of the subduction slab, and the ratios of these elements can
534 be used as reasonable proxy to characterise the nature of the mantle wedge of a particular
535 volcano in the SZ setting (e.g., Pearce, 1983; Pearce and Peate, 1995).
536 Several trace element characteristics of the studied Chikurachki melt inclusions allow us
537 to conclude that the composition of the mantle wedge is similar or even more depleted than the
538 source of typical N-MORB magmas. They are following: (*i*) the average N-MORB-normalised
539 concentrations of $[Nb]_n = 0.55 \pm 0.21$, $[Sm]_n = 1.16 \pm 0.37$, $[Zr]_n = 0.74 \pm 0.30$, $[Ti]_n = 0.74 \pm$
540 0.27, $[Yb]_n = 0.83 \pm 0.29$ are close to, or lower, than unity; (*ii*) the element ratios Zr/Nb = 35–49,
541 Zr/Yb = 16–25, and Nb/Yb = 0.35–0.7 are similar to those of N-MORB (i.e., Zr/Nb = 32, Zr/Yb
542 = 24, Nb/Yb = 0.76; Hofmann, 1988); (*iii*) the studied melt inclusions plot in the field of MORB
543 in the Pearce and Peate (1995) Zr/Yb vs. Nb/Yb discrimination diagram (not shown). Thus, to
544 simplify our calculations, we assume the trace element concentrations of the Kurile arc mantle

545 wedge is the same as depleted N-MORB mantle of Salters and Stracke (2004) (**Table 1**). We
546 note that using more depleted composition of the mantle wedge will not significantly change the
547 calculation results, but slightly increase a role of the slab-derived components.
548
549 *5.3.2. Subduction slab melt vs. fluid as a volatile transport media*
550 The origin of arc magmas is tightly related to dehydration and/or melting of the slab,
551 where both melt and fluid components are added in different proportions, namely higher
552 proportion of fluid at shallower depths and *vice versa* when the slab penetrates deeper (Hickey
553 and Frey, 1982; Cameron, 1985; Tatsumi et al., 1986; Crawford et al., 1989; Eliott et al., 1997).
554 Experiments on element partitioning confirm that slab-derived H_2O-rich fluids may cause
555 remarkable enrichment by incompatible elements typical for volcanic arcs worldwide (e.g.,
556 Brenan et al., 1995; Ayers et al., 1997; Stalder et al., 1998; Johnson and Plank, 1999). Silica-rich
557 partial melts released from the subducting crust and/or sediment are also potential contributors to
558 the chemical balance (Defant and Drummond, 1990; Drummond and Defant, 1990).
559 Several studies proposed a concurrent addition of slab-derived melt and fluid components
560 in the arc magmas (e.g., Kay, 1978; Rogers et al., 1985; Stern et al., 1984; Defant et al., 1991;
561 Stern and Kilian, 1996; Class et al., 2000; Yogodzinski et al., 2001). In particular, it has been
562 concluded that hydrous fluids released in the arc front due to amphibole and serpentine
563 dehydration are enriched in boron, LILE, sulphur and chlorine and likely represent a main fluid
564 transport and reaction agent affecting mantle wedge of the Kurile and Kamchatka arcs (e.g.,
565 Hochstaedter et al., 1996; Ishikawa and Tera, 1997; Churikova et al., 2001, 2007; Portnyagin et
566 al., 2007). Moreover, Churikova et al. (2007) concluded that S, Cl and B could have been
567 transported by a fluid released from AOC-like subduction slab at shallow depth, whereas Li
568 appeared to be related to Li-F-rich fluids resulting from breakdown of volatile-rich minerals
569 (e.g., amphibole) at much greater depths (~400 km). Furthermore, Churikova et al. (2007) have
570 noted that some Kurile-Kamchatka arc magmas may also exhibit an adakitic signature, whereas

571 Portnyagin et al. (2015) argued that melting of the mantle wedge beneath Tolbachik was
572 triggered by slab-derived hydrous melts.

573 We think that in the case of Chikurachki, the significant positive correlations of H_2O/K_2O
574 vs. Cl/K_2O and F/Zr vs. Cl/Nb (**Fig. 5E,F**), Th/Nb vs. Ba/Nb (R = 0.649; see **Fig. 9** and
575 discussion below), as well as B/Nb vs. Li/Nb and Be/Nb (R = 0.833 and 0.796, respectively,
576 except for one outlier; **Fig. S2.2** – *Supporting online material*) imply a complex nature of the
577 Kurile arc subduction component composed of both melt and fluid. The observed strong
578 correlations of Li/Nb and Be/Nb with B/Nb and F/Zr with Cl/Nb in the Chikurachki melt
579 inclusions suggest that these elements have a common source (i.e., slab component), support a
580 major role of a Cl-rich fluid and imply that B, Cl and F are likely to relate to a single transport
581 process, in contrast to the mechanism of B and Li decoupling suggested by Churikova et al.
582 (2007).

583

584 *5.3.3. Trace element constraints*

585 Thorium and LREE are enriched in the subducted slab, being however less mobile or
586 nearly immobile in the fluid phase, as compared to fluid-mobile elements, such as Li, B, Ba, Pb
587 and Sr. The difference in geochemical behaviour of these elements can be used to elucidate a
588 contribution of slab-derived melts vs. dehydration fluids in the origin of arc magmas (e.g.,
589 Kamenetsky et al., 1997; Class et al., 2000; Hochstaedter et al., 2001). Namely, the transport by
590 fluid would leave Th/Nb ratios virtually unchanged since both elements are immobile but affect
591 the ratios of fluid-mobile to fluid-immobile elements (e.g., Ba/Nb, B/Nb), and *vice versa*, if the
592 element transport would have been caused solely by the slab-derived melt. Systematic variations
593 of Th/Nb vs. Ba/Nb or B/Nb ratios would imply the contribution of both slab-derived melt and
594 fluid components.

595 We modelled the contribution of the anticipated subduction sediment-derived melt and
596 fluid components to the mantle wedge following the approach of Hochstaedter et al. (2001). The

AOC- and SED-derived fluids, as well as a partial melt from SED were considered as possible end-members (**Table 2**). The element partitioning data used in the modelling are from experimentally-determined bulk sediment-melt, sediment-fluid, rutile-melt and rutile-fluid partition coefficients (Brenan et al. 1994, 1995; Stalder et al., 1998; Johnson and Plank, 1999; Foley et al., 2000). The sediment subducted at the Kurile trench (its composition is taken from Plank and Langmuir, 1998) is thought to contain up to 5% Ti-rich residual phase (i.e. rutile), which has the potential to fractionate Nb from Th (Class et al., 2000), whereas 1% rutile was assigned for AOC (Hochstaedter et al., 2001). Equilibrium batch melting and Rayleigh fractionation equations (Shaw, 1970) were used to calculate the compositions of partial melt and fluid in equilibrium with the subduction sediment, respectively. We assumed 5% partial melting of the Kurile sediment to produce a sediment melt mixing end-member, and 2% fluid removal from both the Kurile sediment and AOC to account for a possible sediment fluid end-member (**Fig. 10**). We note also that because Ba, Nb and Th are chemical elements of very similar incompatibility to minerals composing magma source rocks, as follows from their solid-melt partition coefficients, they show little or no fractionation during partial melting and/or magma fractionation. The calculated Ba/Nb and Th/Nb ratios of the multi-component magma source region are thus relevant for the Th/Nb and Ba/Nb of the produced partial melts, and can be used to assess the origin of the Chikurachki parental magmas.

In the model presented in **Fig. 10**, the Th/Nb vs. Ba/Nb variations observed in the Chikurachki melt inclusions (presented alongside whole-rock chemical compositions of the Kurile arc mafic lavas) can be explained by partial melting of a magma source composed of the following three components (**Table 2**):

1. A mantle wedge (*MW*) component with trace element concentrations of depleted mantle after Salters and Stracke (2004).

2. A composite dehydration fluid, which is enriched in Ba relative to Th or Nb and presents a 9:1 mixture of the fluid released from the altered oceanic crust (*AOCFluid*, the composition is taken from Hochstaedter et al., 2001) and a fluid produced by dehydration of a subduction sediment (*SedFluid*), whose trace element composition was calculated from that of the Kurile sediment after Plank and Langmuir (1998) (for more detail see explanatory notes in **Table 2**). The 9:1 proportion of *AOCFluid* to *SedFluid* was selected arbitrary, given a subordinate amount of the sediment relative to a total mass of the slab, taking also into account that sediment is more volatile-rich, as compared to its basaltic and ultramafic counterparts. We note however that variations of *AOCFluid* to *SedFluid* ratio do not affect significantly the calculation results.
3. A sediment-derived melt (*SedMelt*) with slightly elevated Th/Nb ratios and significantly lower Ba/Nb ratios, as compared *AOCFluid* and *SedFluid* mixing end-members, whose trace element composition was also calculated from the composition of the Kurile sediment (see also explanatory notes in **Table 2**).

As it follows from our calculations, the composition of subduction component (*SUBD*) is variable. It ranges from the composition of the pure *SedMelt* component (representing a lower limit of the range) to that of *SedMelt* mixed with up to 60% composite slab-derived fluid presenting, in turn, a 9:1-mixture of *AOCFluid* and *SedFluid*, crudely corresponding to the AOC to SED proportion in the dehydrating model slab (Tonarini et al., 2011) and assuming also equal amount of fluid released from both lithologies. The ~1–8% admixture of *SUBD* to *MW* appeared to satisfactorily explain the entire compositional range of the Chikurachki melt inclusions, and from ~0.4% to ~10% of *SUBD* to be mixed with *MW* to account for the range of the Kurile arc magmas **(Fig. 10)**. In conclusion, it is worth emphasising that the subduction component contributed to the origin of the Tolbachik magmas (Portnyagin et al., 2015) appeared to be very similar to *SUBD* inferred during the present study (**Fig. 9; Table 2**).

5.3.4. Implications for chemical composition and amount of slab-derived fluid

Here we evaluate a possible contribution of slab-derived fluid to the origin of volatile components and boron in the studied magmas, assessing the observed B-isotope range. The light lithophile element boron is a powerful proxy to trace fluid transport of chemical elements from subducting slab to the mantle wedge because of strongly contrasting B concentrations and δ^{11}B values in these geochemical reservoirs. A significant fraction of initial boron is contained in the uppermost few km of the subducting crust and sediments, being then progressively released as subduction proceeds (e.g., Leeman and Sisson, 1996). Systematically higher δ^{11}B values in the volcanic arc magmas, as compared to the exhumed subduction-related metamorphic rocks, suggest that dehydration reactions cause significant decrease of δ^{11}B values of subducted crustal material, implying strong fractionation of ^{10}B and ^{11}B isotopes as boron partitions in the fluid (e.g., Peacock and Hervig, 1999). This conclusion was supported by later experimental study of Wunder et al. (2005), who have demonstrated that a wide range of δ^{11}B in the arc magmas may result from continuous breakdown of micas, if they are present in the down-dragged slab. Finally, a serpentinised mantle wedge at the slab-mantle interface represents another major inventory of boron, being also a source of variable but generally positive δ^{11}B values (e.g., Benton et al., 2001; Straub and Layne, 2002; Savov et al., 2005, 2007; Scambelluri and Tonarini, 2012).

Boron mobilised from the slab was shown to be systematically enriched in ^{11}B than the parental AOC at 400–500°C, resulting in +5 to +10‰ enrichment of the fluid relative to the solid (Ishikawa and Nakamura, 1992; Leeman and Sisson, 1996; Rose et al. 2001; Rosner et al. 2003; Leeman et al., 2004; Le Voyer et al., 2008). Since the composition of slab-derived fluid may vary strongly, depending on the composition of subducting crust and the degree of its devolatilisation, a wide δ^{11}B range from –7‰ up to +15‰ (assuming +10‰ enrichment of the

673 fluid phase relative to the upper end of the δ^{11}B range given for AOC by Smith et al., 1997) is
674 very probable (Rose et al. 2001; Leeman et al., 2004; Gurenko et al., 2005b; Le Voyer et al.,
675 2008; Tonarini et al., 2011, Scambelluri and Tonarini, 2012).

676 The effects of possible interaction of slab-derived fluids with depleted MORB-like
677 mantle source are illustrated in diagrams in coordinates of δ^{11}B vs. B/Nb and Ba/Nb ratios (**Fig.**
678 **11**). Given the $^{11}B/^{10}B$, B/Nb and Ba/Nb do not change significantly during partial melting or
679 magma fractionation, these ratios, being calculated for the magma source, can be directly
680 transferred to the resulting partial melts. The following mixing end-members were defined
681 (**Table 1**):

682

683 1. Mantle wedge (*MW*) was chosen to contain 1.2 µg/g Ba, 0.21 µg/g Nb, 0.06 µg/g B and
684 δ^{11}B = –4‰ (Chaussidon and Marty, 1995; Salters and Stracke, 2004).
685 2. Subducting slab fluid (SSF) varies significantly in chemical composition, depending on
686 the particular chemical and lithological composition of the slab and the dehydration
687 depth. In particular, Tonarini et al. (2011) have demonstrated that slab-derived fluids
688 released at the depth range from 30 to 120 km may contain from ~10 and ~200 µg/g B
689 and vary between –10 to higher than +20‰ δ^{11}B. Three contrasting fluid compositions
690 (SSF1 through SSF3) were compiled based on the data of Hochstaedter et al. (2001),
691 Rose et al. (2001), Straub and Layne (2002), Rosner et al. (2003), Leeman et al. (2004),
692 Gurenko et al. (2005b), Le Voyer et al. (2008), Tonarini et al. (2011), Scambelluri and
693 Tonarini (2012), using also the compositions of SED and AOC-derived fluids calculated
694 during the present study (SSF1: trace elements concentrations are those as of *SEDFluid*,
695 containing 300 µg/g B and δ^{11}B = +15‰; SSF2 is the 9:1 mixture of *AOCFluid* and
696 *SedFluid* as calculated above, containing 100 µg/g B and δ^{11}B = +3‰; and SSF3 is equal
697 to *AOCFluid* with 50 µg/g B and δ^{11}B = –8‰). The decrease of B and Ba contents and

698 δ^{11}B values in the fluid components qualitatively reflects the increase of slab temperature
699 and degree of its devolatilisation.
700
701 As it follows from the calculations, the slab-derived fluid may represent a major agent affecting
702 the abundances of volatile and fluid-mobile elements, and B isotopes in the melt inclusions.
703 About 1–10% of SSF2 and SSF3 have to be added to MW in order to explain the ~9‰ range of
704 δ^{11}B values of the studied melt inclusions. We note that this estimation is very similar to that
705 inferred from the trace element modelling (1 to 8% addition of SUBD; **Fig. 9**). It is also worth
706 emphasising that the selected compositions of SSF2 and SSF3 are very close to the model fluid
707 compositions released from the South Sandwich Island arc uppermost slab at 90–120 km depth
708 (170–190 µg/g B and δ^{11}B = –0.7 to –3.9‰; Tonarini et al., 2011), but having less boron and
709 more negative δ^{11}B values. This discrepancy can be explained by somewhat stronger dehydration
710 of the residual Kurile slab because of the greater depth of the Wadati-Benioff zone beneath
711 Chikurachki (~130–140 km; e.g., Ishikawa and Tera, 1997; Ishikawa et al., 2001).
712
713 *5.4. Magma assent, degassing history and eruption style*
714 It is well known that conduit geometry, magma viscosity, degassing history, changing
715 conditions of magma ascent and fragmentation, and even the dynamics of syn-eruptive microlite
716 growth may strongly affect the eruption rate and style of a volcano (e.g., Fischer and Schmincke,
717 1984; Carey and Sparks, 1986; Houghton et al., 2004; Szramek et al., 2006, 2010; Houghton and
718 Gonnermann, 2008). Previously, Gurenko et al. (2005a) suggested intensive pre-eruptive
719 degassing of H_2O and S from the magma at the stage of phenocryst crystallisation, pointing on
720 the strongly varying to very low volatile contents in the melt inclusions trapped by phenocrysts
721 of the same or very close chemical composition. The authors suggested a scenario by which local
722 volumes of magma could be partially degassed before being trapped by growing crystals and

723 employed a mechanism of vertical cycling of magma within one or between several connected
724 reservoirs, being akin to the magma drainback phenomenon described in particular for Kilauea
725 Volcano, Hawaii (e.g., Wallace and Anderson, 1998). Our present data (i.e., numerous
726 correlations of volatile component concentrations and S isotope compositions preserved in the
727 studied melt inclusions with incompatible trace elements and between each other, inability of
728 magma degassing and crustal contamination to account for these variations coupled with the
729 suggested here two-component mixing scenario to explain δ^{34}S vs. S concentrations) could be
730 interpreted in support of the mechanism previously suggested by Gurenko et al. (2005a) to
731 control the variations of H_2O, S, Cl and F in the erupting magmas.
732 The required insignificant correction of melt inclusion compositions for post-entrapment
733 crystallisation of host mineral (i.e., less than 7.8 wt.% Ol, 0.8 wt.% Opx, and no correction for
734 Pl) also suggests that the eruption and quenching of magma likely occurred shortly after the
735 inclusions have been entrapped by growing phenocrysts. As previously discussed (e.g.,
736 Roggensack et al., 1997; Gurenko et al., 2005a; Shinohara, 2008; Ruth et al., 2016), eventual
737 eruptions may be non-explosive, if magma degassing is effective at shallow crustal depth,
738 whereas rapid ascent of a volatile-rich magma may result in strong volatile release and highly
739 explosive character of eruptions. In this context, the range of volatile contents recorded by melt
740 inclusions and their relationships with other chemical components may indicate whether the
741 erupted magma underwent a prolonged stage of relatively passive degassing or degassing was
742 essentially a single-stage process upon the eruption. It is worth emphasising that most of the
743 historic eruptions from Chikurachki have been of the non-explosive character, possibly linked to
744 the episodes where volatile components were able to dissipate smoothly. Explosive eruptions, in
745 contrast, are thought to occur when access to shallow levels is blocked or when the flux of
746 magma from depth is too rapid for shallow degassing to prevent a catastrophic decompression
747 and explosive fragmentation of the magma. We thus think that rapid ascent of the volatile-rich

748 basaltic magmas from ~16-km initial depth (inferred from our CO_2-H_2O data; **Fig. 4B**) was a
749 primary reason caused the Plinian character of the Chikurachki eruptions.
750
751 **6. Summary and conclusions**
752 The present study focuses on the unravelling the origin and behaviour of volatile
753 components resulting in highly explosive (Plinian) basaltic eruptions of the Chikurachki volcano.
754 The following main conclusions were derived:
755
756 1. The obtained concentrations of volatile components in the studied melt inclusions agree well
757 with our previously reported data. After correction for post-entrapment crystallisation of the
758 host mineral, the concentrations of CO_2 and H_2O reveal minimum pressure of 33 to 276 MPa
759 (or ~9.5 to ~1 km depth), corresponding to the last equilibrium between melt and vapour
760 phases upon magma eruption and quenching. About 5–69% of the original CO_2 and
761 0.1–3.2% of H_2O were lost to the shrinkage bubble of melt inclusions after their entrapment
762 during phenocryst crystallisation. After correction, the obtained 47–1580 μg/g CO_2, 0.4–4.2
763 wt.% H_2O, 399–633 μg/g F, 619–3402 μg/g S and 805–1240 μg/g Cl ranges imply strong
764 pressure release from 456 to 35 MPa, corresponding to ~15.7–1.2-km-depth range of magma
765 ascent.
766 2. Significant negative correlations of S with incompatible trace elements, no clear relationships
767 of S with H_2O, CO_2 and Cl but strong positive correlations of S/K_2O with H_2O/K_2O, Cl/K_2O
768 and F/K_2O suggest that later magma degassing and/or contamination by crustal rocks were
769 not the governing processes affecting the amounts of S and probably of the other volatile
770 components preserved in inclusions
771 3. Sulphur isotopes in the studied inclusion and groundmass glasses vary strongly, ranging from
772 –1.6 to +12.3‰ of $\delta^{34}S$, decrease with decreasing S concentrations and show significant

positive correlations with H_2O, CO_2 and S, as well as negative correlations with light lithophile (Li, Be and B), and with a number of incompatible trace elements. Our modelling has demonstrated that either open- or close-system magma degassing cannot account for the observed ~14‰ range of $\delta^{34}S$ variations in the Chikurachki melt inclusions. The linear character of the 1/S vs. $\delta^{34}S$ relationship suggests mixing of two components possibly represented by melts having similar major and trace element compositions but strongly contrasting volatile contents and S isotopes.

4. The $\delta^{11}B$ values of the studied melt inclusions range from −7.0 to +2.4‰ within the interval of B concentrations of 13–23 μg/g. Similarly, the relationships of $\delta^{11}B$ with B/K_2O and B/Nb, as well as of Cl/K_2O with B/K_2O (and equally, Cl/Nb with B/Nb) cannot be accounted by magma contamination at shallow crustal depths.

5. The observed relationships of S/K_2O with K_2O-normalised concentrations of H_2O, Cl and F, as well as the H_2O/K_2O vs. Cl/K_2O and F/Zr vs. Cl/Nb correlations strongly suggest that variations in H_2O, S, Cl and F contents were not primarily affected by degassing or contamination, but likely originated due to the mixing of magmas, which in turn reflect the composition of source components. We contend that subduction slab-derived melt and/or fluid were major agents in controlling chemical and isotopic composition of the mantle wedge and, consequently, of the magmas originated from this hybrid source.

6. The behaviour of fluid-mobile vs. fluid-immobile incompatible trace elements points towards strongly varying chemical composition of the subduction component. It ranges from the composition of the pure subducted sediment-derived melt (a lower limit of the range) to that of the sediment melt mixed with up to 60% composite slab-derived fluid, representing in turn a 9:1-mixture of fluid components released from both altered oceanic crust and the sediment of the slab. The ~1–8% admixture of the inferred subduction component to the mantle wedge is required to account for the whole compositional range of the studied Chikurachki magmas,

and addition from ~0.4% to ~10% of the subduction component accounts for the broad compositional range of the Kurile arc magmas.

7. We conclude that rapid ascent of the volatile-rich basaltic magmas from ~16-km initial depth without their prolonged stagnation and crystallisation in shallower depth magma reservoir but accompanied by near-surface bubble nucleation and growth followed by magma fragmentation was a primary reason caused Plinian character of the Chikurachki eruptions.

Acknowledgements

We thank Peter Landry for his help and ensuring stable working conditions of the NENIMF CAMECA IMS 1280 instrument, Charlie Mandeville and Alberto Saal for fruitful discussions, Anastassia Borisova for review and comments of the early manuscript version. The insightful reviews, useful comments and suggestions, as well as a thorough correction of English by John Caulfield and two anonymous referees are very much appreciated. This work was benefited from the NENIMF financial support of AAG during his training as a SIMS research specialist, the NSF grant EAR 0911093 to AAG, and partially from the Russian Science Foundation grant #16-17-10145 to VSK and MEZ. This is CRPG contribution *#24??*

816 **References**

817 Alt, J.C., Shanks III, W.C., Jackson, M.C., 1993. Cycling of sulfur in subduction zones: The
818 geochemistry of sulfur in the Mariana Island Arc and back-arc trough. Earth and Planetary
819 Science Letters 119, 477–494.

820 Anderson, A.T., 1974. Chlorine, sulfur and water in magmas and oceans. Bulletin of Geological
821 Society of America 85, 1485–1492.

822 Arculus, R.J., Powell, R., 1986. Source component mixing in the regions of arc magma
823 generation. Journal of Geophysical Research 91, 5913–5926.

824 Aster, E.M., Wallace, P.J., Moore, L.R., Watkins, J., Gazel, E., Bodnar, R.J., 2016.
825 Reconstructing CO_2 concentrations in basaltic melt inclusions using Raman analysis of
826 vapor bubbles. Journal of Volcanology and Geothermal Research 323, 148–162.

827 Ayers J.C., Dittmer, S.K., Layne G., 1997. Partitioning of elements between peridotite and H_2O
828 at 2.0–3.0 GPa and 900–1100°C, and application to models of subduction zone processes.
829 Earth and Planetary Science Letters 150, 381–398.

830 Bailey, J.C., Frolova, T.I., Burikova, I.A., 1987a. Mineralogy, geochemistry and petrogenesis of
831 Kurile Island Arc basalts. Contribution to Mineralogy and Petrology 102, 265–280.

832 Bailey, J.C., Larsen, O., Frolova, T.I., 1987b. Strontium isotope variations in lower Tertiary-
833 Quaternary volcanic rocks from the Kurile Island Arc. Contribution to Mineralogy and
834 Petrology 95, 155–165.

835 Belousov, A.B., Belousova, M.G., Grushin, S.Yu., Krestov, P.B., 2003. Historic eruptions of the
836 Chikurachki volcano (Paramushir, Kurile Islands). Volcanology and Seismology 3, 15-34
837 (in Russian).

838 Belousov, A., Belousova, M., Edwards, B., Volynets, A., Melnikov, D., 2015. Overview of the
839 precursors and dynamics of the 2012–13 basaltic fissure eruption of Tolbachik Volcano,
840 Kamchatka, Russia. Journal of Volcanology and Geothermal Research 307, 22-37.

841 Belousov, A., Belousova, M., Kozlov, D. 2017. Distribution of tephra deposit and reconstruction
842 of parameters of the 1973 explosive eruption of Tyatya volcano, Kunashir Island, Kuriles.
843 Volcanology and Seismology, in print (in Russian).
844 Benton, L.D., Ryan, J.G., Tera, F., 2001. Boron isotope systematics of slab fluids as inferred
845 from a serpentine seamount, Mariana forearc, Earth and Planetary Science Letters 187,
846 273–282.
847 Bernard, A., Demaiffe, D., Mattielli, N., Punanongbayan, R.S., 1991. Anhydrite-bearing pumices
848 from Mount Pinatubo: further evidence for the existence of sulfur-rich silicic magmas.
849 Nature 354, 139–140.
850 Bindeman, I.N., Ponomareva, V.V., Bailey, J.C., Valley, J.W., 2004. Volcanic arc of
851 Kamchatka: a province with high-$\delta^{18}O$ magma sources and large-scale $^{18}O/^{16}O$ depletion of
852 the upper crust. Geochimica et Cosmochimica Acta 68, 841–865.
853 Brasseur, G., Granier, C., 1992. Mount Pinatubo aerosols, chlorofluorocarbons and ozone
854 depletion. Science 257, 1239−1242.
855 Brenan, J.M., Shaw, H.F., Phinney, D.L., Ryerson, F.J., 1994. Rutile-aqueous fluid partitioning
856 of Nb, Ta, Hf, Zr, U and Th: implications for high field strength element depletions in
857 island-arc basalts. Earth and Planetary Science Letters 128, 327–339.
858 Brenan, J.M., Shaw, H.F., Ryerson, F.J., Phinney, D.L., 1995. Mineral-aqueous fluid partitioning
859 of trace elements at 900°C and 2.0 GPa: constraints on the trace element chemistry of mantle
860 and deep crustal fluids. Geochimica et Cosmochimica Acta 59, 3331–3350.
861 Burgisser, A., Scaillet, B., 2007. Redox evolution of a degassing magma rising to the surface.
862 Nature 445, 194–197.
863 Cabral, R.A., Jackson, M.G., Koga, K.T., Rose-Koga, E.F., Hauri, E.H., Whitehouse, M.J., Price,
864 A.A., Day, J.M.D., Shimizu, N., Kelley, K.A., 2014. Volatile cycling of H_2O, CO_2, F, and Cl

865 in the HIMU mantle: A new window provided by melt inclusions from oceanic hot spot
866 lavas at Mangaia, Cook Islands. Geochemistry Geophysics Geosystems 15, 4445–4467.
867 Cameron, W.E., 1985. Petrology and origin of primitive lavas from the Troodos ophiolite,
868 Cyprus. Contribution to Mineralogy and Petrology 89, 239–255.
869 Canil, D., Fellows, S.A., 2017. Sulphide–sulphate stability and melting in subducted sediment
870 and its role in arc mantle redox and chalcophile cycling in space and time. Earth and
871 Planetary Science Letters 470, 73–86.
872 Carey, S., Sparks, R.S.J., 1986. Quantitative models of the fallout and dispersal of tephra from
873 volcanic eruption columns. Bulletin of Volcanology 48, 109–125.
874 Carroll, M.R., Rutherford, M.J., 1985. Sulfide and sulfate saturation in hydrous silicate melts.
875 Journal of Geophysical Research 90, C601–C612.
876 Carroll, M.R., Rutherford, M.J., 1987. The stability of igneous anhydrite: experimental results
877 and implications for sulfur behavior in the 1982 El Chichon trachyandesite and other
878 evolved magmas. Journal of Petrology 28, 781–801.
879 Carroll, M.R., Rutherford, M.J., 1988. Sulfur speciation in hydrous experimental glasses of
880 varying oxidation state: results from measured wavelength shifts of sulfur X-ray. American
881 Mineralogist 73, 845–849.
882 Carroll, M.R., Webster, J.D., 1994. Solubilities of sulfur, noble gases, nitrogen, chlorine, and
883 fluorine in magmas, in: Carroll, M.R., Holloway, J.R. (Eds.), Volatiles in Magmas, Reviews
884 in Mineralogy 30, Mineralogical Society of America, Washington DC, pp 231–279.
885 Caulfield, J.T., Cronin, S.J., Turner, S.P., Cooper, L.B., 2011. Mafic Plinian volcanism and
886 ignimbrite emplacement at Tofua volcano, Tonga. Bulletin of Volcanology 73, 1259–1277.
887 Chaussidon, M., Jambon, A., 1994. Boron content and isotopic composition of oceanic basalts:
888 geochemical and cosmochemical implications. Earth and Planetary Science Letters 121,
889 277–291.

Chaussidon, M., Marty, B., 1995. Primitive boron isotope composition of the mantle. Science, 269, 383–386.

Chaussidon, M., Albarède, F., Sheppard, S.M.F., 1987. Sulphur isotope heterogeneity in the mantle from ion microprobe measurements of sulphide inclusions in diamonds. Nature 330, 242–244.

Churikova T., Dorendorf F., Wörner G., 2001. Sources and fluids in the mantle wedge below Kamchatka, evidence from across-arc geochemical variation. Journal of Petrology 42, 1567–1593.

Churikova, T., Wörner, G., Mironov, N., Kronz, A., 2007. Volatile (S, Cl and F) and fluid mobile trace element compositions in melt inclusions: implications for variable fluid sources across the Kamchatka arc. Contributions to Mineralogy and Petrology 154, 217–239.

Class, C., Miller, D.M., Goldstein, S.L., Langmuir, C.H., 2000. Distinguishing melt and fluid subduction components in Umnak Volcanics, Aleutian Arc. Geochemistry Geophysics Geosystems 1, 1999GC000010.

Connolly, J.W.D., Haughton, D.R., 1972. The valence of sulfur in glass of basaltic composition formed under low oxidation potential. American Mineralogist 57, 1515–1517.

Crawford, A.J., Falloon, T.J., Green, D.H., 1989. Classification, petrogenesis and tectonic setting of boninites, in: Crawford, A.J. (Ed.), Boninites. Unwin Hyman, London, pp. 1–49.

Dalou, C., Koga, K.T., Le Voyer, M., Shimizu, N., 2014. Contrasting partition behaviour of F and Cl during hydrous mantle melting: implications for Cl/F signature in arc magmas. Progress in Earth and Planetary Science 1, 26.

Davidson, J.P., 1987. Crustal contamination versus subduction zone enrichment: examples from the Lesser Antilles and implications for mantle source composition of island arc volcanic rocks. Geochimica et Cosmochimica Acta 51, 2185–2198.

914 Defant, M.J., Drummond, M.S., 1990. Derivation of some modern arc magmas by melting of
915 young subducted lithosphere. Nature 347, 662–665.
916 Defant, M.J., Richerson, P.M., De Boer, J.Z., Stewart, R.H., Maury, R.C., Bellon, H.,
917 Drummond, M.S., Feigenson, M.D., Jackson, T.E., 1991. Dacite genesis via both slab
918 melting and differentiation: Petrogenesis of La Yeguada volcanic complex, Panama. Journal
919 of Petrology 32, 1101–1142.
920 Ding, T., Valkiers, S., Kipphardt, H., De Bièvre, P., Taylor, P.D.P., Gonfiantini, R., Krouse, R.,
921 2001. Calibrated sulfur isotope abundance ratios of three IAEA sulfur isotope reference
922 materials and V-CDT with a reassessment of the atomic weight of sulfur. Geochimica et
923 Cosmochimica Acta 65: 2433–2437.
924 Dorendorf, F., Wiechert, U., Wörner, G., 2000. Hydrated sub-arc mantle: a source for the
925 Kluchevskoy volcano, Kamchatka/Russia. Earth and Planetary Science Letters 175, 69–86.
926 Drummond, M.S., Defant, M.J., 1990. A model for trondhjemite-tonalite-dacite genesis and
927 crustal growth via slab melting: Archaean to modern comparisons. Journal of Geophysical
928 Research 95, 503–521.
929 Elliott, T., Plank, T., Zindler, A., White, W., Bourdon, B., 1997. Element transport from slab to
930 volcanic front at the Mariana arc. Journal of Geophysical Research 102, 14991–15019.
931 Esposito, R., Bodnar, R.J., Danyushevsky, L.V., De Vivo, B., Fedele, L., Hunter, J., Lima, A.,
932 Shimizu, N., 2011. Volatile evolution of magma associated with the Solchiaro eruption in
933 the Phlegrean Volcanic District (Italy). Journal of Petrology 52, 2431–2460.
934 Fedotov, S.A., Markhinin, Ye.K., 1983. The Great Tolbachik Fissure Eruption. Cambridge Univ.
935 Press, New York.
936 Fiege, A., Holtz, F., Behrens, H., Mandeville, C.W., Shimizu, N., Crede, L.S., Göttlicher, J.,
937 2015. Experimental investigation of the S and S-isotope distribution between H2O-S ± Cl
938 fluids and basaltic melts during decompression. Chemical Geology 393–394, 36–54.

939 Fisher, R.V., Schmincke, H.-U., 1984. Pyroclastic rocks. Springer-Verlag, Berlin, Heidelberg,
940 New York, Tokyo.
941 Foley, S.F., Barth, M.G., Jenner, G.A., 2000. Rutile/melt partition coefficients for trace elements
942 and an assessment of the influence of rutile on the trace element characteristics of
943 subduction zone magmas. Geochimica et Cosmochimica Acta 64, 933–938.
944 Francis, P., 1993. Volcanoes: a planetary perspective. Clarendon Press, Oxford.
945 Gill, J.B., 1981. Orogenic andesites and plate tectonics. Springer-Verlag, Berlin-Heidelberg.
946 Gill, J., Torssander, P., Lapierre, H., Taylor, R., Kaiho, K., Koyama, M., Kusakabe, M.,
947 Aitchison, J., Cisowski, S., Dadey, K., Fujioka, K., Klaus, A., Lovell, M., Marsaglia, K.,
948 Pezard, P., Taylor, B., Tazaki, K., 1990. Explosive deep-water basalt in the Sumisu Backarc
949 Rift. Science 248, 1214−1217.
950 Gorshkov, G.S., 1967. Volcanism of the Kurile Island Arc. Nauka, Moscow (in Russian).
951 Gurenko, A.A., Chaussidon, M., 1997. Boron concentrations and isotopic composition in the
952 Icelandic mantle: evidence from glass inclusions in olivine. Chemical Geology 135, 21–34.
953 Gurenko, A.A., Kamenetsky, V.S., 2011. Boron isotopic composition of olivine-hosted melt
954 inclusions from Gorgona komatiites, Colombia: New evidence supporting wet komatiite
955 origin. Earth and Planetary Science Letters 312, 201–212.
956 Gurenko, A.A., Schmincke, H.-U., 2000. S concentrations and its speciation in Miocene basaltic
957 magmas north and south of Gran Canaria (Canary Islands): Constraints from glass inclusions
958 in olivine and clinopyroxene. Geochimica et Cosmochimica Acta 64, 2321–2337.
959 Gurenko, A.A., Chaussidon, M., Schmincke, H.-U., 2001. Magma ascent and contamination
960 beneath one intraplate volcano: Evidence from S and O isotopes in glass inclusions and their
961 host clinopyroxenes from Miocene basaltic hyaloclastites southwest of Gran Canaria
962 (Canary Islands). Geochimica et Cosmochimica Acta 65, 4359−4374.

963 Gurenko, A.A., Belousov, A.B., Trumbull, R.B., Sobolev, A.V., 2005a. Explosive basaltic
964 volcanism of the Chikurachki Volcano (Kurile arc, Russia): Insights on pre-eruptive
965 magmatic conditions and volatile budget revealed from phenocryst-hosted melt inclusions
966 and matrix glasses. Journal of Volcanology and Geothermal Research 147, 203–232.
967 Gurenko, A.A., Trumbull, R.B., Thomas, R., Lindsay J.M., 2005b. A melt inclusion record of
968 volatiles, trace elements and Li-B isotope variations in a single magma system from the Plat
969 Pays Volcanic Complex, Dominica, Lesser Antilles. Journal of Petrology 46, 2495–2526.
970 Hartley, M.E., Maclennan, J., Edmonds, M., Thordarson, T., 2014. Reconstructing the deep CO_2
971 degassing behaviour of large basaltic fissure eruptions. Earth and Planetary Science Letters
972 393, 120–131.
973 Hasegawa, T., Nakagawa, M., Yoshimoto, M., Ishizuka, Y., Hirose, W., Seki, S. I., Ponomareva,
974 V., Alexander, R., 2011. Tephrostratigraphy and petrological study of Chikurachki and Fuss
975 volcanoes, western Paramushir Island, northern Kurile Islands: Evaluation of Holocene
976 eruptive activity and temporal change of magma system. Quaternary International 246,
977 278–297.
978 Haughton, D.R., Roeder, P.L., Skinner, B.J., 1974. Solubility of sulfur in mafic magmas.
979 Economic Geology 69, 541–567.
980 Hawkesworth, C.J., Gallagher K., Hergt J. M., and McDermott F. (1993) Mantle and slab
981 contributions in arc magmas. Annual Review of Earth and Planetary Sciences 21, 175–204.
982 Hickey, R.L., Frey, F.A., 1982. Geochemical characteristics of boninite series volcanics:
983 Implications for their source. Geochimica et Cosmochimica Acta 46, 2099–2115.
984 Hickey, R., Frey, F.A., Gerlach, D.C., Lopez-Escobar, L., 1986. Multiple sources for basaltic arc
985 rocks from the southern volcanic zone of the Andes (34°–41°S): Trace element and isotopic
986 evidence for contributions from subducted oceanic crust, mantle and continental crust.
987 Journal of Geophysical Research 91, 5963–5983.

988 Hochstaedter, A.G., Kepezhinskas, P., Defant, M., 1996. Insights into volcanic arc mantle wedge
989 from magnesian lavas from the Kamchatka arc. Journal of Geophysical Research 101,
990 697–712.
991 Hochstaedter, A., Gill, J., Peters, R., Broughton, P., Holden, P., Taylor, B., 2001. Across-arc
992 geochemical trends in the Izu-Bonin arc: Contributions from the subducting slab.
993 Geochemistry Geophysics Geosystems 2, 2000GC000105.
994 Hofmann, A.W., 1988. Chemical differentiation of the Earth: the relationship between mantle,
995 continental crust and oceanic crust. Earth and Planetary Science Letters 90, 297–314.
996 Holloway, J.R., Blank, J.G., 1994. Application of experimental results to C-O-H species in
997 natural melts, in: Carroll, M.R., Holloway, J.R. (Eds.), Volatiles in Magmas. Reviews in
998 Mineralogy 30, Mineralogical Society of America, Washington, D.C., pp. 187–230.
999 Houghton, B.F., Gonnermann, H.M., 2008. Basaltic explosive volcanism: Constraints from
1000 deposits and models. Chemie der Erde 68, 117–140.
1001 Houghton, B.F., Wilson, C.J.N., Del Carlo, P., Coltelli, M., Sable, J.E., Carey, R., 2004. The
1002 influence of conduit processes on changes in style of basaltic Plinian eruptions: Tarawera
1003 1886 and Etna 122 BC. Journal of Volcanology and Geothermal Research 137, 1–14.
1004 Ikeda, Y., 1998. Geochemistry of Miocene back-arc basin basalts from northeast Hokkaido,
1005 Japan. The Journal of the Geological Society of Japan 104, 99–106.
1006 Ikeda, Y., Stern, R.J., Kagami, H., Sun, C.-H., 2000. Pb, Nd, and Sr isotopic constraints on the
1007 origin of Miocene basaltic rocks from northeast Hokkaido, Japan: implications for opening
1008 of the Kurile back-arc basin. Island Arc 9, 161–172.
1009 Ishikawa, T., Nakamura, E., 1992. Boron isotope geochemistry of the oceanic crust from
1010 DSDP/ODP hole 504B. Geochimica et Cosmochimica Acta 56, 1633–1639.

1011 Ishikawa, T., Tera, F., 1997. Source, composition and distribution of the fluid in the Kurile
1012 mantle wedge: constraints from across-arc variations of B/Nb and B isotopes. Earth and
1013 Planetary Science Letters 152, 123–138.
1014 Ishikawa, T., Tera, F., Nakazawa, T., 2001. Boron isotope and trace element systematics of the
1015 three volcanic zones in the Kamchatka arc. Geochimica et Cosmochimica Acta 65,
1016 4523–4537.
1017 Jambon, A. 1994. Earth degassing and large-scale geochemical cycling of volatile elements, in:
1018 Carroll, M.R., Holloway, J.R. (Eds.), Volatiles in Magmas. Reviews in Mineralogy 30,
1019 Mineralogical Society of America, Washington, D.C., pp 479–517.
1020 Jambon, A., Déruelle, B., Dreibus, G., Pineau, F., 1995. Chlorine and bromine abundance in
1021 MORB: the contrasting behaviour of the Mid-Atlantic Ridge and East Pacific Rise and
1022 implications for chlorine geodynamic cycle. Chemical Geology 126, 101–117.
1023 Johnson, M.C., Plank, T., 1999. Dehydratation and melting experiments constrain the fate of
1024 subducted sediments. Geochemistry Geophysics Geosystems 1, 1999GC000014.
1025 Jugo, P.J., Luth, R.W., Richards, J.P., 2005a. An experimental study of the sulfur content in
1026 basaltic melts saturated with immiscible sulfide or sulfate Liquids at 1300°C and 1.0 GPa.
1027 Journal of Petrology 46, 783–798.
1028 Jugo, P.J., Luth, R.W., Richards, J.P., 2005. Experimental data on the speciation of sulfur as a
1029 function of oxygen fugacity in basaltic melts. Geochimica et Cosmochimica Acta 69,
1030 497–503.
1031 Jugo, P.J., Wilke, M., Botcharnikov, R.E., 2010. Sulfur K-edge XANES analysis of natural and
1032 synthetic basaltic glasses: Implications for S speciation and S content as function of oxygen
1033 fugacity. Geochimica et Cosmochimica Acta 74, 5926–5938.
1034 Kamenetsky, V.S., Crawford, A.J., Eggins, S., Mühe, R., 1997. Phenocryst and melt inclusion
1035 chemistry of near-axis seamounts, Valu Fa Ridge, Lau basin: insight into mantle wedge

melting and the addition of subduction components. Earth and Planetary Science Letters 151, 205–223.

Katsura, T., Nagashima, S., 1974. Solubility of sulfur in some magmas at 1 atmosphere. Geochimica et Cosmochimica Acta 38, 517–531.

Kay, R.W., 1978. Aleutian magnesian andesites: melts from subducted Pacific ocean crust. Journal of Volcanology and Geothermal Research 4, 117–132.

Kendrick, M.A., Arculus, R., Burnard, P., Honda, M., 2013. Quantifying brine assimilation by submarine magmas: Examples from the Galápagos Spreading Centre and Lau Basin. Geochimica et Cosmochimica Acta 123, 150–165.

Kent, A.J.R., Norman, M.D., Hutcheon, I.D., Stolper, E.M., 1999. Assimilation of seawater-derived components in an oceanic volcano: evidence from matrix glasses and glass inclusions from Loihi seamount, Hawaii. Chemical Geology 156, 299–319.

Kepezhinskas, P., McDermott, F., Defant, M.J., Hochstaedter, A., Drummond, M.S., Hawkesworth, C., Koloskov, A., Maury, R.C., Bellon, H., 1997. Trace element and Sr-Nd-Pb isotopic constraints on a three-component model of Kamchatka Arc petrogenesis. Geochimica et Cosmochimica Acta 61, 577–600.

Khubunaya, S.A., Sobolev, A.V., 1998. Primary melts of calc-alkaline magnesian basalts from the Klyuchevskoi volcano, Kamchatka. Doklady Akademii Nauk 360, 100–102.

Konrad-Schmolke, M., Halama, R., Manea, V.C., 2016. Slab mantle dehydrates beneath Kamchatka – Yet recycles water into the deep mantle. Geochemistry Geophysics Geosystems 17, 2987–3007.

Kress, V., 1997. Magma mixing as a source for Pinatubo sulphur. Nature 389, 591–593.

Langmuir, C.H., Vocke, R.D., Hanson, G.N., Hart, S.R. (1978). A general mixing equation with applications to Icelandic basalts. Earth and Planetary Science Letters 37, 380–392.

1060 Lassiter, J.C., Hauri, E.H., Nikogosian, I.K., Barsczus, H.G., 2002. Chlorine-potassium
1061 variations in melt inclusions from Raivavae and Rapa, Austral Islands: Constraints on
1062 chlorine recycling in the mantle and evidence for brine-induced melting of oceanic crust.
1063 Earth and Planetary Science Letters 202, 525–540.
1064 Leeman, W.P., Sisson, V.B., 1996. Geochemistry of boron and its implications for crustal and
1065 mantle processes, in: Grew, E.S., Anovitz, L.M. (Eds.), Boron: Mineralogy, Petrology and
1066 Geochemistry. Mineralogical Society of America 33, Washington, D.C., pp. 645–707.
1067 Leeman, W.P., Tonarini, S., Chan, L.H., Borg, L.E., 2004. Boron and lithium isotopic variations
1068 in a hot subduction zone—the southern Washington Cascades. Chemical Geology 212,
1069 101−124.
1070 Le Voyer, M., Rose-Koga, E.F., Laubier, M., Schiano, P., 2008. Petrogenesis of arc lavas from
1071 the Rucu Pichincha and Pan de Azucar volcanoes (Ecuadorian arc): Major, trace element,
1072 and boron isotope evidences from olivine-hosted melt inclusions. Geochemistry Geophysics
1073 Geosystems 9, doi: 12010.11029/12008GC002173.
1074 Le Voyer, M., Cottrell, E., Kelley, K.A., Brounce, M., Hauri, E.H., 2015. The effect of primary
1075 versus secondary processes on the volatile content of MORB glasses: an example from the
1076 equatorial Mid-Atlantic Ridge (5°N–3°S). Journal of Geophysical Research 120,
1077 2014JB011160.
1078 le Roux, P.J., Shirey, S.B., Hauri, E.H., Perfit, M.R., Bender, J.F., 2006. The effects of variable
1079 sources, processes and contaminants on the composition of northern EPR MORB (8–10°N
1080 and 12–14°N): Evidence from volatiles (H_2O, CO_2, S) and halogens (F, Cl). Earth and
1081 Planetary Science Letters 251, 209–231.
1082 Luhr, J.F., 1990. Experimental phase relations of water and sulfur saturated arc magmas and the
1083 1982 eruptions of El Chichón volcano. Journal of Petrology 31, 1071−1114.

1084 Luhr, J.F., Carmichael, I.S.E., Varekamp, J.C., 1984. The 1982 eruptions of El Chichón
1085 Volcano, Chiapas, Mexico: mineralogy and petrology of the anhydrite-bearing pumices.
1086 Journal of Volcanology and Geothermal Research 23, 69–108.
1087 Macpherson, C.G., Mattey, D.P., 1998. Oxygen isotope variations in Lau Basin lavas. Chemical
1088 Geology 144, 177–194.
1089 Mandeville, C.W., Webster, J.D., Tappen, C., Taylor, B.E., Timbal, A., Sasaki, A., Hauri, E.,
1090 Bacon, C.R., 2009. Stable isotope and petrologic evidence for open-system degassing during
1091 the climactic and pre-climactic eruptions of Mt. Mazama, Crater Lake, Oregon. Geochimica
1092 et Cosmochimica Acta 73, 2978–3012.
1093 Marini, L., Moretti, R., Accornero, M., 2011. Sulfur isotopes in magmatic-hydrothermal
1094 systems, melts, and magmas. Reviews in Mineralogy and Geochemistry 73, 423–492.
1095 Mathez, E.A., 1976. Sulfur solubility and magmatic sulfides in submarine basalt glasses. Journal
1096 of Geophysical Research 81, 4269–4276.
1097 Mavrogenes, J.A., O'Neill, H.S.C., 1999. The relative effects of pressure, temperature and
1098 oxygen fugacity on the solubility of sulfide in mafic magmas. Geochimica et Cosmochimica
1099 Acta 63, 1173–1180.
1100 Mavrogenes, J., Blundy, J., 2017. Crustal sequestration of magmatic sulfur dioxide. Geology 45,
1101 211–214.
1102 Matjuschkin, V., Blundy, J.D., Brooker, R.A., 2016. The effect of pressure on sulphur speciation
1103 in mid- to deep-crustal arc magmas and implications for the formation of porphyry copper
1104 deposits." Contributions to Mineralogy and Petrology 171, 66.
1105 McCulloch, M.T., Gamble, J.A., 1991. Geochemical and geodynamical constraints on
1106 subduction zone magmatism. Earth and Planetary Science Letters 102, 358–374.
1107 Metrich, N., Clocchiatti R., 1996. Sulfur abundance and its speciation in oxidized alkaline melts.
1108 Geochimica et Cosmochimica Acta 60, 4151–4160.

1109 Métrich, N., Schiano, P., Clocchiatti, R., Maury, R.C., 1999. Transfer of sulfur in subduction
1110 settings: an example from Batan Island (Luzon volcanic arc, Philippines). Earth and
1111 Planetary Science Letters 167, 1–14.
1112 Michael, P.J., Cornell, W.C., 1998. Influence of spreading rate and magma supply on
1113 crystallisation and assimilation beneath mid-ocean ridges: Evidence from chlorine and major
1114 element chemistry of mid-ocean ridge basalts. Journal of Geophysical Research 103,
1115 18325–18356.
1116 Michael, P., Schilling, J.-G., 1989. Chlorine in mid-ocean ridge magmas: evidence for
1117 assimilation of seawater-influenced components. Geochimica et Cosmochimica Acta 53,
1118 3131–3143.
1119 Mironov, N., Portnyagin, M., Botcharnikov, R., Gurenko, A., Hoernle, K., Holtz, F., 2015.
1120 Quantification of the CO_2 budget and H_2O–CO_2 systematics in subduction-zone magmas
1121 through the experimental hydration of melt inclusions in olivine at high H_2O pressure. Earth
1122 and Planetary Science Letters 425, 1–11.
1123 Moore, L.R., Gazel, E., Tuohy, R., Lloyd, A.S., Esposito, R., Steele-MacInnis, M., Hauri, E.H.,
1124 Wallace, P.J., Plank, T., Bodnar, R.J., 2015. Bubbles matter: An assessment of the
1125 contribution of vapor bubbles to melt inclusion volatile budgets. American Mineralogist
1126 100, 806–823.
1127 Miyoshi, T., Sakai, H., Chiba, H., 1984. Experimental study of sulfur isotope fractionation
1128 factors between sulfate and sulfide in high temperature melts. Geochemical Journal 18, 75–
1129 84.
1130 Newman, S., Lowenstern, J.B., 2002. VolatileCalc: a silicate melt-H_2O-CO_2 solution model
1131 written in Visual Basic for Excel. Computers and Geosciences 28, 597–604.
1132 Ovsyannikov, A.A., Muravyev, Y.D., 1992. Eruptions of the Chikurachki volcano. Volcanology
1133 and Seismology 5-6, 3−21 (in Russian).

1134 Peacock, S.M., Hervig, R.L., 1999. Boron isotopic composition of subduction-zone metamorphic
1135 rocks. Chemical Geology 160, 281–290.
1136 Pearce, J.A., 1983. Role of the sub-continental lithosphere in magma genesis at active
1137 continental margins, in: Hawkesworth, C.J., Norry, M.J. (Eds.), Continental Basalts and
1138 Mantle Xenoliths. Shiva Publishing, Nantwich, UK, pp. 230–249.
1139 Pearce, J.A., Peate, D.W., 1995. Tectonic implications of the composition of volcanic arc
1140 magmas. Annual Review of Earth and Planetary Sciences 24, 251–285.
1141 Plank, T., Langmuir, C.H., 1998. The chemical composition of subducting sediment and its
1142 consequences for the crust and mantle. Chemical Geology 145, 325−394.
1143 Portnyagin, M., Hoernle, K., Plechov, P., Mironov, N., Khubunaya, S., 2007. Constraints on
1144 mantle melting and composition and nature of slab components in volcanic arcs from
1145 volatiles (H_2O, S, Cl, F) and trace elements in melt inclusions from the Kamchatka Arc.
1146 Earth and Planetary Science Letters 255, 53–69.
1147 Portnyagin, M., Duggen, S., Hauff, F., Mironov, N., Bindeman, I., Thirlwall, M., Hoernle, K.,
1148 2015. Geochemistry of the late Holocene rocks from the Tolbachik volcanic field,
1149 Kamchatka: quantitative modelling of subduction-related open magmatic systems. Journal
1150 of Volcanology and Geothermal Research 307, 133–155.
1151 Richet, P., Bottinga, Y., Javoy, M., 1977. A review of hydrogen, carbon, nitrogen, oxygen, sulfur
1152 and chlorine stable isotope fractionation among gaseous molecules. Annual Review of Earth
1153 and Planetary Sciences 5, 65–110.
1154 Robin, C., Eissen, J.P., Monzier, M., 1993. Giant tuff cone and 12-km-wide associated caldera at
1155 Ambrym Volcano (Vanuatu, New Hebrides Arc). Journal of Volcanology and Geothermal
1156 Research 55, 225−238.

1157 Roggensack, K., Hervig, R.L., McKnight, S.B., Williams, S.N., 1997. Explosive basaltic
1158 volcanism from Cerro Negro volcano: Influence of volatiles on eruptive style. Science 277,
1159 1639−1642.
1160 Rogers, G., Saunders, A.D., Terrell, D.J., Verma, S.P., Marriner, G.F., 1985. Geochemistry of
1161 Holocene volcanic rocks associated with ridge subduction in Baja, California, Mexico.
1162 Nature 315, 389−392.
1163 Rose, E.F., Shimizu, N., Layne, G.D., Grove, T.L., 2001. Melt production beneath Mt. Shasta
1164 from boron data in primitive melt inclusions. Science 293, 281−283.
1165 Rosner, M., Erzinger, J., Franz, G., Trumbull, R.B., 2003. Slab-derived boron isotope signatures
1166 in arc volcanic rocks from the Central Andes and evidence for boron isotope fractionation
1167 during progressive slab dehydration. Geochemistry Geophysics Geosystems 4, doi:
1168 0.1029/2002GC000438.
1169 Ruth, D.C.S., Cottrell, E., Cortés, J.A., Kelley, K.A., Calder, E.S., 2016. From passive degassing
1170 to violent strombolian eruption: the case of the 2008 eruption of Llaima volcano, Chile.
1171 Journal of Petrology 57, 1833−1864.
1172 Ryan, J.G., Langmuir, C.H., 1993. The systematics of boron abundances in young volcanic
1173 rocks. Geochimica et Cosmochimica Acta 57, 1489−1498.
1174 Ryan, J.G., Morris, J., Tera, F., Leeman, W.P., Tsvetkov, A., 1995. Cross-arc geochemical
1175 variations in the Kurile Arc as a function of slab depth. Science 270, 625−627.
1176 Saal, A.E., Hauri, E.H., Langmuir, C.H., Perfit, M.R., 2002. Vapour undersaturation in primitive
1177 mid-ocean-ridge basalt and the volatile content of Earth's upper mantle. Nature 419,
1178 451−455.
1179 Sable, J.E., Houghton, B.F., Del Carlo, P., Coltelli, M., 2006. Changing conditions of magma
1180 ascent and fragmentation during the Etna 122 BC basaltic Plinian eruption: Evidence from
1181 clast microtextures. Journal of Volcanology and Geothermal Research 158, 333−354.

1182 Sakai, H., Casadevall, T.J., Moore, J.G., 1982. Chemistry and isotopic ratios of sulfur in basalts
1183 and volcanic gases at Kilauea volcano, Hawaii. Geochimica et Cosmochimica Acta 46, 729–
1184 738.
1185 Sakai, H., Des Marais, D.J., Ueda, A., Moore, J.G., 1984. Concentrations and isotope ratios of
1186 carbon, nitrogen and sulfur in ocean floor basalt. Geochimica et Cosmochimica Acta 48,
1187 2433–2441.
1188 Salters, V.J.M., Stracke, A., 2004. Composition of the depleted mantle. Geochemistry
1189 Geophysics Geosystems 5, doi: 10.1029/2003GC000597.
1190 Savov, I.P., Ryan, J.G, D'Antonio, M., Kelley, K., Mattie, P., 2005. Geochemistry of
1191 serpentinized peridotites from the Mariana Forearc-Conical Seamount, ODP Leg 125:
1192 Implications for the elemental recycling at subduction zones. Geochemistry Geophysics
1193 Geosystems 6, Q04J15, doi: 10.1029/2004GC000777.
1194 Savov, I.P., Ryan, J.G., D'Antonio, M., Fryer, P., 2007. Shallow slab fluid release across and
1195 along the Mariana arc-basin system: Insights from geochemistry of serpentinized peridotites
1196 from the Mariana Forearc. Journal of Geophysical Research 112, doi:
1197 10.1029/2006JB004749.
1198 Scambelluri, M., Tonarini, S., 2012. Boron isotope evidence for shallow fluid transfer across
1199 subduction zones by serpentinized mantle. Geology 40, 907–910.
1200 Selvaraja, V., Fiorentini, M.L., LaFlamme, C.K., Wing, B.A., Bui, T.-H., 2017. Anomalous
1201 sulfur isotopes trace volatile pathways in magmatic arcs. Geology 45, 419–422.
1202 Shaw, D.M., 1970. Trace element fractionation during anatexis. Geochimica et Cosmochimica
1203 Acta 34, 237–243.
1204 Shimizu, K., Shimizu, N., Komiya, T., Suzuki, K., Maruyama, S., Tatsumi, Y., 2009. CO_2-rich
1205 komatiitic melt inclusions in Cr-spinels within beach sand from Gorgona Island, Colombia.
1206 Earth and Planetary Science Letters 288, 33–43.

1207 Simons, K., Dixon, J., Schilling, J.-G., Kingsley, R., Poreda, R., 2002. Volatiles in basaltic
1208 glasses from the Easter-Salas y Gomez Seamount Chain and Easter Microplate: Implications
1209 for geochemical cycling of volatile elements. Geochemistry Geophysics Geosystems 3, doi:
1210 10.1029/2001GC000173.
1211 Shinohara, H., 2008. Excess degassing from volcanoes and its role on eruptive and intrusive
1212 activity. Reviews of Geophysics 46, RG4005, doi: 10.1029/2007RG000244.
1213 Smith, H.J., Leeman, W.P., Davidson, J., Spivack, A.J., 1997. The B isotopic composition of arc
1214 lavas from Martinique, Lesser Antilles. Earth and Planetary Science Letters 146, 303–314.
1215 Smythe, D.J., Wood, B.J., Kiseeva, E.S., 2017. The S content of silicate melts at sulfide
1216 saturation: New experiments and a model incorporating the effects of sulfide composition.
1217 American Mineralogist 102, 795–803.
1218 Spivack, A.J., Edmond, J.M., 1986. Determination of boron isotope ratios by thermal ionization
1219 mass spectrometry of the dicesium metaborate cation. Analytical Chemistry 58, 31–35.
1220 Soto, G.J., Alvarado G.E., 2006. Eruptive history of Arenal Volcano, Costa Rica, 7 ka to present.
1221 Journal of Volcanology and Geothermal Research 157, 254–269.
1222 Stalder, R., Foley, S.F., Brey, G.P., Horn, I., 1998. Mineral-aqueous fluid partitioning of trace
1223 elements at 900–1200°C and 3.0–5.7 GPa: new experimental data for garnet, clinopyroxene,
1224 and rutile, and implications for mantle metasomatism. Geochimica et Cosmochimica Acta
1225 62, 1781–1801.
1226 Staudigel, H., Plank, T., White, B., Schmincke, H.-U., 1996. Geochemical fluxes during seafloor
1227 alteration of the basaltic upper oceanic crust: DSDP Sites 417 and 418, in: Bebout, G.E.,
1228 Scholl, D.W., Kirby, S.H., Platt, J.P. (Eds.), Subduction: Top to Bottom. Geophysical
1229 Monography 96, American Geophysical Union, pp. 19–38.

1230 Steele-Macinnis, M., Esposito, R., Bodnar, R.J., 2011. Thermodynamic model for the effect of
1231 post-entrapment crystallization on the H_2O–CO_2 systematics of vapor-saturated, silicate melt
1232 Inclusions. Journal of Petrology 52, 2461–2482.
1233 Stern, C.R., Kilian, R., 1996. Role of the subducted slab, mantle wedge and continental crust in
1234 the generation of adakites from the Andean Austral Volcanic Zone. Contribution to
1235 Mineralogy and Petrology 123, 263–281.
1236 Stern, C.R., Futa, K., Muehlenbachs, K., 1984. Isotope and trace element data for orogenic
1237 andesites from the Austral Andes, in: Harmon, R.S., Barreiro, B.A. (Eds.), Andean
1238 Magmatism: Chemical and Isotopic Constraints. Shiva Publishing, Cheshire, UK, pp.
1239 31–46.
1240 Straub, S.M., Layne G.D., 2002. The systematics of boron isotopes in Izu arc front volcanic
1241 rocks. Earth and Planetary Science Letters 198, 25–39.
1242 Straub, S.M., Layne, G.D., 2003. The systematics of chlorine, fluorine, and water in Izu arc front
1243 volcanic rocks: Implications for volatile recycling in subduction zones. Geochimica et
1244 Cosmochimica Acta 67, 4179–4203.
1245 Symonds, R.B., Rose, W.I., Bluth, G.J.S., Gerlach, T.M., 1994. Volcanic-gas studies: methods,
1246 results, and applications, in: Carroll, M.R., Holloway, J.R. (Eds.), Volatiles in Magmas.
1247 Reviews in Mineralogy 30, Mineralogical Society of America, Washington, D.C., pp 1–66.
1248 Szramek, L., Gardner, J.E., Larsen, J., 2006. Degassing and microlite crystallization of basaltic
1249 andesite magma erupting at Arenal Volcano, Costa Rica. Journal of Volcanology and
1250 Geothermal Research 157, 182–201.
1251 Takagi, T., Orihashi, Y., Naito, K., Watanabe, Y., 1999. Petrology of a mantle-derived rhyolite,
1252 Hokkaido, Japan. Chemical Geology 160, 425–445.
1253 Tatsumi, Y., Hamilton, D.L., Nesbitt, R.W., 1986. Chemical characteristics of fluid phase
1254 released from a subducted lithosphere and origin of arc magmas: evidence from high-

1255 pressure experiments and natural rocks. Journal of Volcanology and Geothermal Research
1256 29, 293–309.
1257 Tatsumi, Y., Furukawa, Y., Kogiso, T., Yamada, Y., Yokoyama, T., Fedotov, S.A., 1994. A third
1258 volcanic chain in Kamchatka: Thermal anomaly at transform/convergence plate boundary.
1259 Geophysical Research Letters 21, 537–540.
1260 Taylor, B.E., 1986. Magmatic volatiles: isotopic variation of C, H, and S, in: Valley, J.W.
1261 Taylor, Jr., H.P., O'Neil, J.R. (Eds.), Stable Isotopes in High Temperature Geological
1262 Processes, Reviews in Mineralogy 16, Mineralogical Society of America, Washington, D.C.,
1263 pp. 185–225.
1264 Thirlwall, M.F., Graham, A.M., Arculus, R.J., Harmon, R.S., Macpherson, C.G., 1996.
1265 Resolution of the effects of crustal assimilation, sediment subduction, and fluid transport in
1266 island arc magmas: Pb-Sr-Nd-O isotope geochemistry of Grenada, Lesser Antilles.
1267 Geochimica et Cosmochimica Acta 60, 4785–4810.
1268 Tonarini, S., Leeman, W.P., Leat, P.T., 2011. Subduction erosion of forearc mantle wedge
1269 implicated in the genesis of the South Sandwich Island (SSI) arc: Evidence from boron
1270 isotope systematics. Earth and Planetary Science Letters 301, 275–284.
1271 Turner, S., Hawkesworth, C., Rogers, N., Bartlett, J., Worthington, T., Hergt, J., Pearce, J.A.,
1272 Smith, I., 1997. ^{238}U-^{230}Th disequilibria, magma petrogenesis, and flux rates beneath the
1273 depleted Tonga-Kermadec island arc. Geochimica et Cosmochimica Acta 61, 4855–4884.
1274 Varekamp, J.C., Luhr, J.F., Prestegaard, K.L., 1984. The 1982 eruptions of El Chichón Volcano
1275 (Chiapas, Mexico): character of the eruptions, ash-fall deposits, and gas phase. Journal of
1276 Volcanology and Geothermal Research 23, 39–68.
1277 Vroon, P.Z., Lowry, D., van Bergen, M.J., Boyce, A.J., Mattey, D.P., 2001. Oxygen isotope
1278 systematics of the Banda Arc: Low δ^{18}O despite involvement of subducted continental
1279 material in magma genesis. Geochimica et Cosmochimica Acta 65, 589–609.

1280 Walker, G.P.L., 1973. Explosive volcanic eruptions – a new classification scheme. Geologische
1281 Rundschau 62, 431−446.
1282 Walker, G.P.L., 1980. The Taupo pumice: product of the most powerful known (ultraplinian)
1283 eruption? Journal of Volcanology and Geothermal Research 8, 69−94.
1284 Walker, G.P.L., Self, S., Wilson, L., 1984. Tarawera 1886, New Zealand — A basaltic plinian
1285 fissure eruption. Journal of Volcanology and Geothermal Research 21, 61−78.
1286 Wallace, P.J., Anderson, A.T.J., 1998. Effects of eruption and lava drainback on the H_2O
1287 contents of basaltic magmas at Kilauea Volcano. Bulletin of Volcanology 59, 327−344.
1288 Wallace, P., Carmichael, I.S.E., 1992. Sulfur in basaltic magmas. Geochimica et Cosmochimica
1289 Acta 56, 1863−1874.
1290 Wallace, P.J., Carmichael, I.S.E., 1994. S speciation in submarine basaltic glasses as determined
1291 by measurements of SK_α X-ray wavelength shifts. American Mineralogist 79, 161−167.
1292 Wallace, P.J., Kamenetsky, V.S. Cervantes, P., 2015. Melt inclusion CO_2 contents, pressures of
1293 olivine crystallization, and the problem of shrinkage bubbles. American Mineralogist 100,
1294 787−794.
1295 Walowski, K.J., Wallace, P.J., Clynne, M.A., Rasmussen, D.J., Weis, D., 2016. Slab melting and
1296 magma formation beneath the southern Cascade arc. Earth and Planetary Science Letters
1297 446, 100−112.
1298 Wilson, L., Walker, G.P.L., 1987. Explosive volcanic eruptions – VI. Ejecta dispersal in plinian
1299 eruptions: the control of eruption conditions and atmospheric properties. Geophysical
1300 Journal of the Royal Astronomical Society 89, 657−679.
1301 Williams, S.N., 1983. Plinian airfall deposits of basaltic composition. Geology 11, 211−214.
1302 Woodhead, J., Eggins, S., Gamble, J., 1993. High field strength and transition element
1303 systematics in island arc and back-arc basin basalts: evidence for multi-phase melt
1304 extraction and a depleted mantle wedge. Earth and Planetary Science Letters 114, 491−504.

1305 Wunder, B., Meixner, A., Romer, R.L., Wirth, R., Heinrich, W., 2005. The geochemical cycle of
1306 boron: Constraints from boron isotope partitioning experiments between mica and fluid.
1307 Lithos 84, 206–216.
1308 Yogodzinski, G.M., Lees, J.M., Churikova, T.G., Dorendorf, F., Wörner, G., Volynets, O.N.,
1309 2001. Geochemical evidence for the melting of subducting oceanic lithosphere at plate
1310 edges. Nature 409, 500–504.
1311
1312

Figure captions

Fig. 1. (A) Schematic map of the northern Kurile Islands (Russia) with the locality of the Chikurachki volcano on Paramushir Island shown in relation to the Kamchatka Peninsula. Contours show isobars for the top of the Wadati-Benioff zone from Tatsumi et al. (1994). (B) The Chikurachki volcano, a view from the eastern side ~6 km away.

Fig. 2. Isopachs (lines of equal thickness) given in cm of the tephra representing Plinian (A) 1853 and (B) 1986 eruptions of the Chikurachki volcano after Belousov et al. (2003).

Fig. 3. Multi-element diagram presenting trace and rare-earth element distribution in olivine-hosted glass inclusions and groundmass glasses and demonstrating positive H_2O, B, Cl and F enrichment. The concentrations of trace elements in N-MORB used for normalisation are from Hofmann (1988), the normalisation values for volatile elements and water are 1350 μg/g H_2O, 0.6 μg/g B, 54.5 μg/g Cl, and 146 μg/g F, which were calculated from the average B/K ≈ 0.001, H_2O/Ce ≈ 180, K/Cl ≈ 11, and F/Nd ≈ 20, or F/Zr ≈ 2 ratios inferred for MORB using the data of Ryan and Langmuir (1993), Jambon et al. (1995), Saal et al. (2002), Kendrick et al. (2013), Le Voyer et al. (2015) and references therein. The shaded field presents whole-rock data for the Kurile island arc basalts and andesites (MgO > 2.5 wt.%) from Bailey et al. (1987a,b), Ishikawa and Tera (1997), Ikeda (1998), Ikeda et al. (2000), Takagi et al. (1999), Ishikawa et al. (2001).

Fig. 4. Concentrations of CO_2 and H_2O dissolved in glass inclusions measured by SIMS. (A) CO_2 and H_2O corrected for the amount of host mineral crystallised inside melt inclusions between entrapment and magma eruption and final quenching. (B) CO_2 and H_2O corrected for the loss of volatiles to the inclusion shrinkage bubble (see text). Isobars of melt compositions in equilibrium with CO_2-H_2O fluid (*solid lines*) and isopleths of fluid composition (dashed lines

with labels returning molecular fraction of H_2O in the fluid) were calculated using *VolatileCalc* solution model (Newman and Lowenstern, 2002). The isopleths and isobars were calculated for basaltic magma composition at 1000°C i.e., the average temperature of the Chikurachki magmas (Gurenko et al., 2005a). *Error bars* represent $\pm 2\sigma$ average integral analytical uncertainty, i.e., ±18% relative for CO_2 and ±12% relative for H_2O, they are less then the size of a symbol, if not shown.

Fig. 5. Concentrations of S, Cl and F in glass inclusions and lapilli matrix glasses. (A) FeO vs. S variations. The larger shaded grey symbols denote the compositions of the respective host matrix glasses. The *MORB and OIB* shaded field presents data for presumably undegassed MORB and Hawaiian submarine tholeiitic and alkali basaltic glasses from Wallace and Carmichael (1992). The *S saturation* shaded field represents compositional dependence of sulphur saturation of MORB-type magmas with immiscible sulfide liquid of pure FeS based on experimental data of Smythe et al. (2017) and references therein. Legend: *MI* = melt inclusions, *GL* = matrix glasses. (B) Ce vs. S, (C) H_2O/K_2O vs. S/K_2O, (D) F/K_2O vs. S/K_2O, (E) H_2O/K_2O vs. Cl/K_2O, and (F) F/Zr vs. Cl/Nb. The observed relationships do not support shallow-depth contamination of the magma, and rather favour a deep origin of volatiles resulted from slab-derived fluid released during subduction (see text).

Fig. 6. Sulphur isotope composition of glass inclusion and one host matrix glass of the Chikurachki prehistoric eruption related to (A) S concentrations, (B) H_2O/K_2O and (C) Cl/K_2O ratios.

Fig. 7. Diagrams of (A) H_2O/K_2O vs. Cl/K_2O, (B) H_2O/Ce vs. Cl/Nb, (C) H_2O/K_2O vs. B/K2O, and (D) H_2O/Ce vs. B/Nb (given as weight ratios) illustrate the effects of contamination (mixing lines) of presumably "uncontaminated" arc magma (*UAM*) with different types of contaminants,

i.e., seawater (*SW*), 15%- and 50%-NaCl saline brines (labelled as *15%-NaCl* and *50%-NaCl*, respectively), altered oceanic crust (*AOC1* and *AOC2*) and siliceous marine sediment (*SED*) (see text and **Table 1** for the end-member chemical compositions and further details). Numbers on the mixing lines refer to wt.% of the contaminant added to the magma. The calculated mixing trends allow us to conclude that direct contamination of UAM by altered basaltic rocks and marine sediments at shallow depth and/or by seawater or seawater-derived components (saline brine) is unable to account for the H_2O, Cl and B enrichment observed in the studied melt inclusions. Legend: *MI* = melt inclusions, *GL* = matrix glasses.

Fig. 8. Boron isotope composition of the studied glass inclusions given in relation to B/K_2O (A) and B/Nb (B) in context of possible magma contamination. The mixing end-members used (and their labels) are the same as in **Fig. 7**. It is demonstrated that magma contamination by seawater or seawater-derived components, altered oceanic crust and marine sediments is unable to account for B isotopic composition of the studied melt inclusions.

Fig. 9. Sulphur isotope fractionation during magma degassing. The $\delta^{34}S$ values in the melt inclusions are shown versus fraction of S remaining (*F*). Shifts of $\delta^{34}S$ were calculated assuming closed-system (equilibrium, solid and dashed *straight lines*) and open-system (Rayleigh distillation; solid and dashed *curves*) degassing (see text), the $\alpha_{gas-melt}$ values of 0.996 and 0.998, and maximum, undegassed S concentration found in the most S-rich melt inclusions having the highest $\delta^{34}S$ values. At the temperature range from 910 to 1180°C and the redox conditions of NNO+1 to NNO+2 obtained for the studied Chikurachki magmas, the outgassed SO_2 will drive out the lighter ^{32}S isotope so that the remaining melt will be progressively enriched in ^{34}S. Thus, degassing alone cannot explain the observed, ~10‰-S-isotope of the studied melt inclusions.

Fig. 10. Diagram Th/Nb vs. Ba/Nb illustrating a possible origin of the Chikurachki magmas as a result of melting of a three-component magma source. Legend: *MI* = melt inclusions, *GL* = matrix glasses. The source components are mantle wedge (*MW*) with Ba, Nb and Th concentrations of the depleted mantle after Salters and Stracke (2004) and hybrid subduction component (*SUBD*) representing a binary 4:6-mixture of a sediment melt (*SedMelt*) with a composite slab-derived fluid, which in turn is a 9:1-mixture of a dehydration fluids released from the altered oceanic crust (*AOCFluid*) and Kurile sediment (*SedFluid*) (see text and **Table 2** for definition). The compositions of *Kurile lavas* are from Bailey et al. (1987a,b), Ishikawa and Tera (1997), Ikeda (1998), Ikeda et al. (2000), Takagi et al. (1999), Ishikawa et al. (2001). *KurileSed* is a bulk composition of the sediment column subducted at the Kurile trench taken from Plank and Langmuir (1998). *AOC* is altered oceanic crust taken from Staudigel et al. (1996), whose composition was used by Hochstaedter et al. (2001) to calculate *AOCFluid* composition. *SlabMelt* is a composition of composite hydrous melt released from the slab and contributed to the origin of magmas erupted in the Tolbachik volcanic field, Kamchatka, which was taken from Portnyagin et al. (2015) for comparison.

Fig. 11. Diagrams of (A) δ^{11}B vs. B/Nb and (B) δ^{11}B vs. Ba/Nb illustrate the proposed interpretation to account for B-isotope variations in the Chikurachki mineral-hosted melt inclusions by addition of slab-derived fluids to the mantle wedge. Mixing lines between the depleted MORB-type mantle wedge (*MW*) and subduction slab fluids (*SSF1*, *SSF2* and *SSF3*) are shown (see **Table 1** for chemical composition). Numbers on mixing lines refer to wt% of component added to MW end-member.

Figure

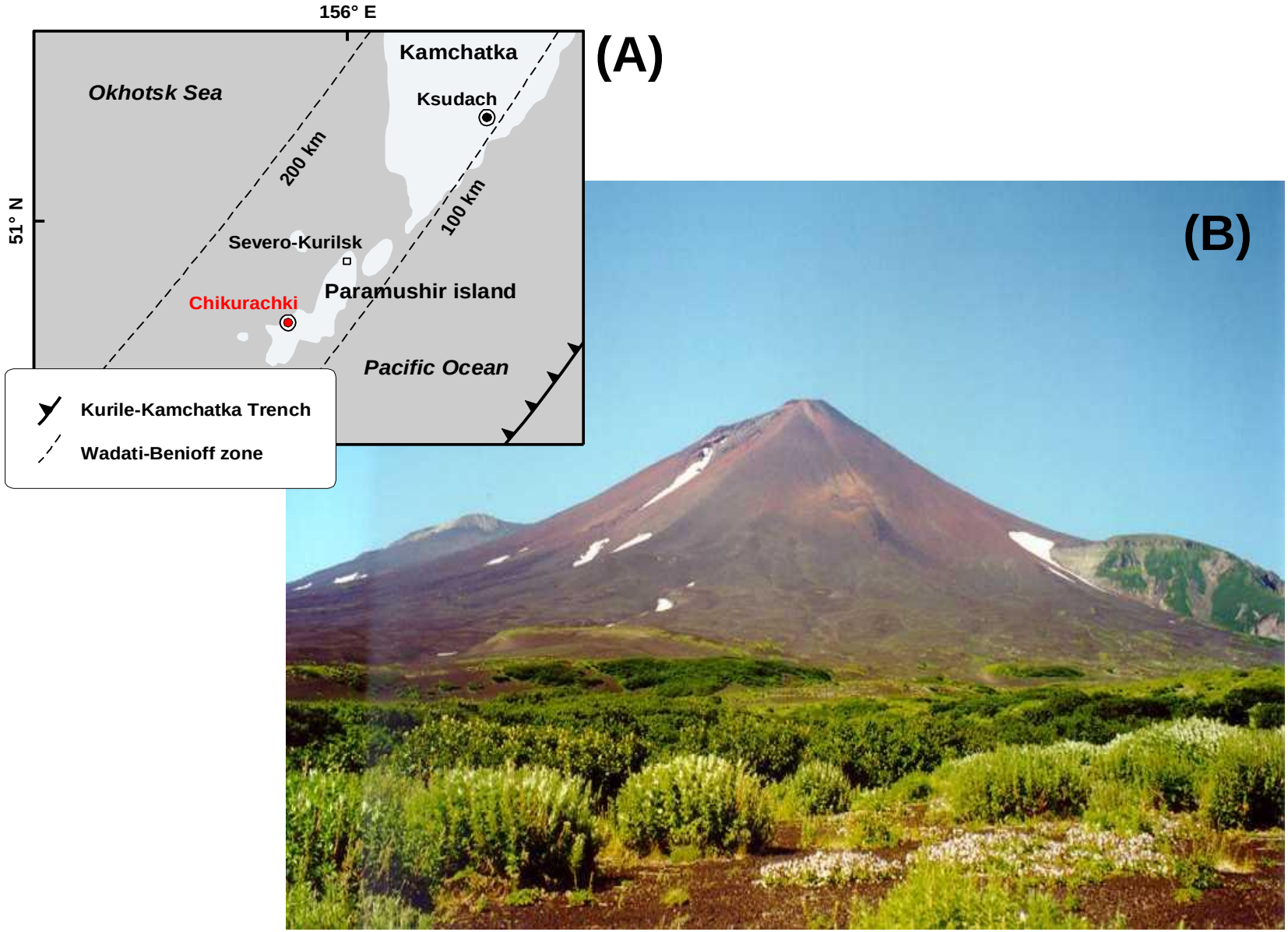

Fig. 1. Gurenko et al.

Figure

(A) 1853 eruption

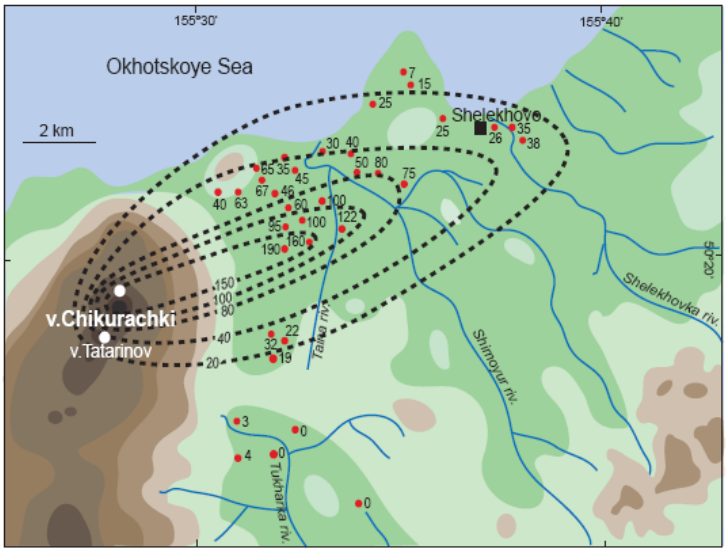

(B) 1986 eruption

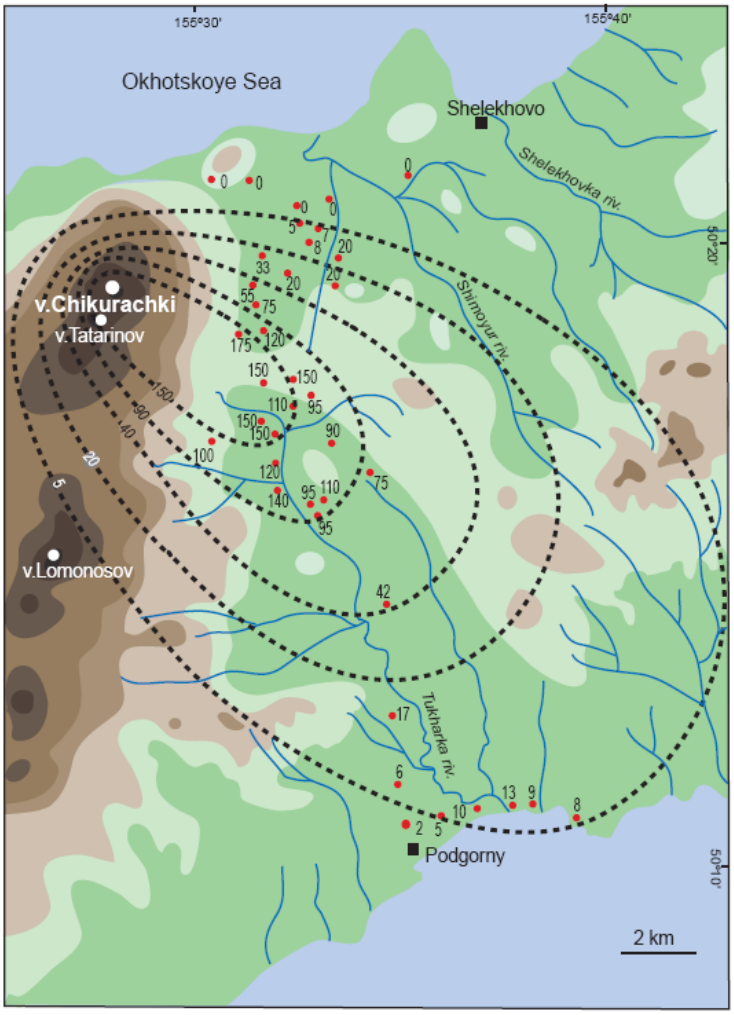

Fig. 2. Gurenko et al.

Figure

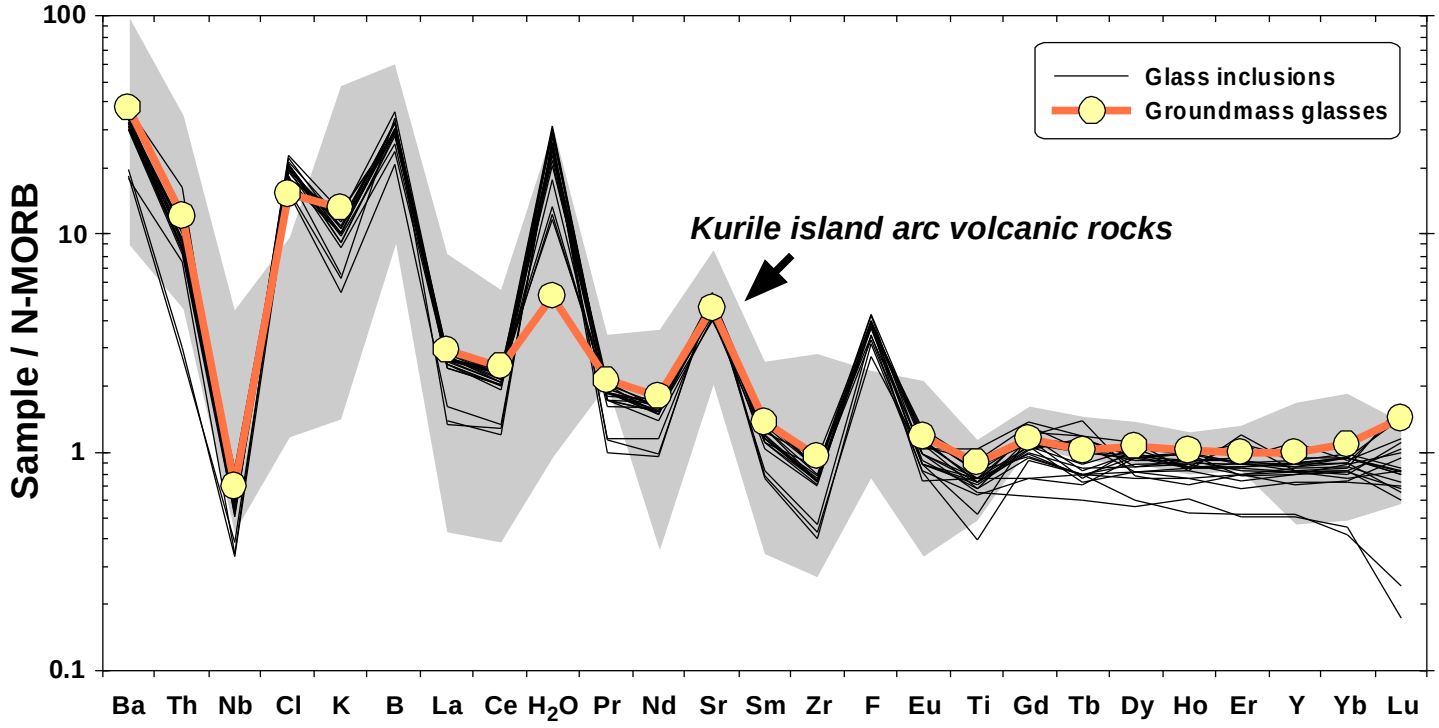

Fig. 3. Gurenko et al.

Figure

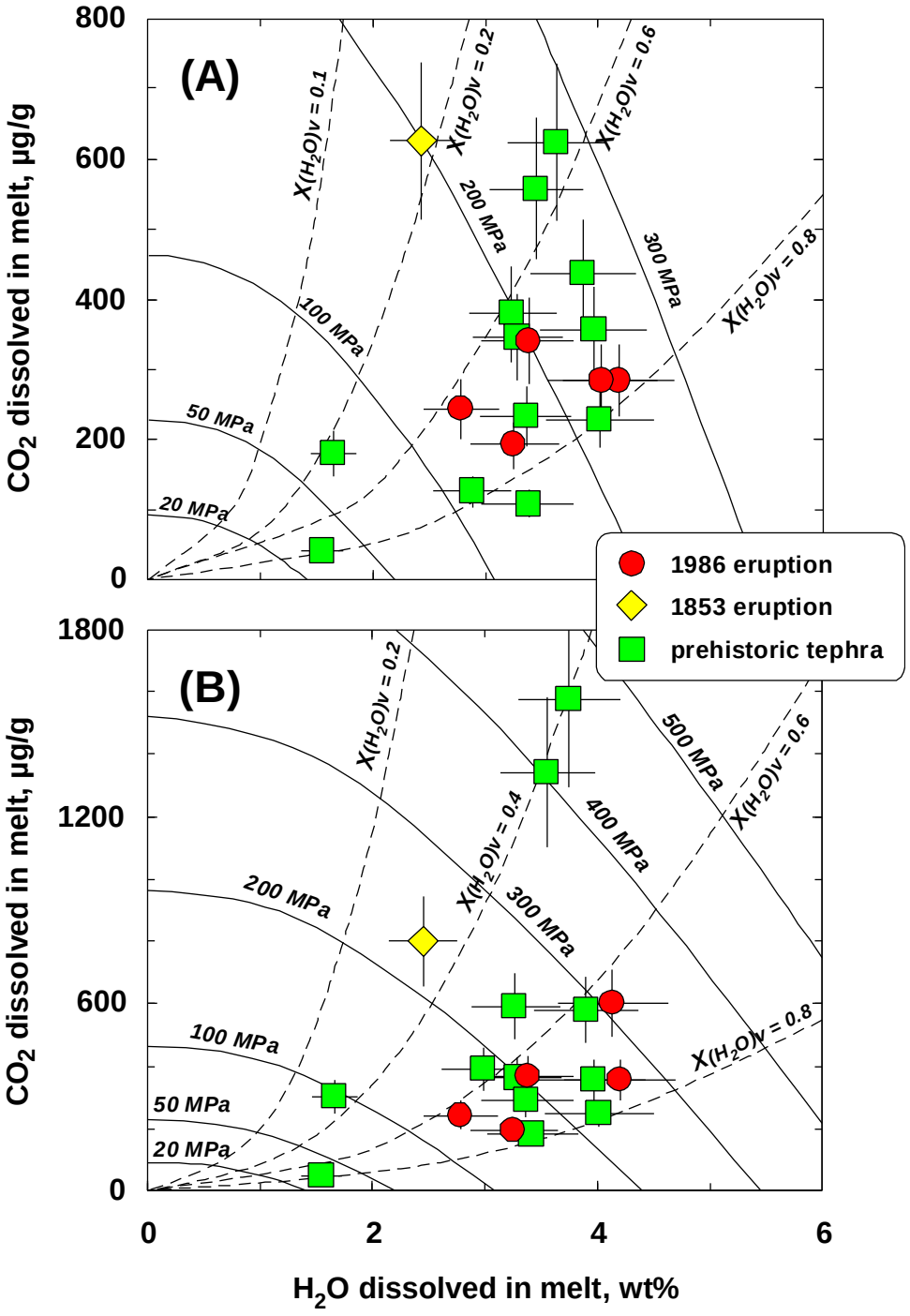

Fig. 4. Gurenko et al.

Figure

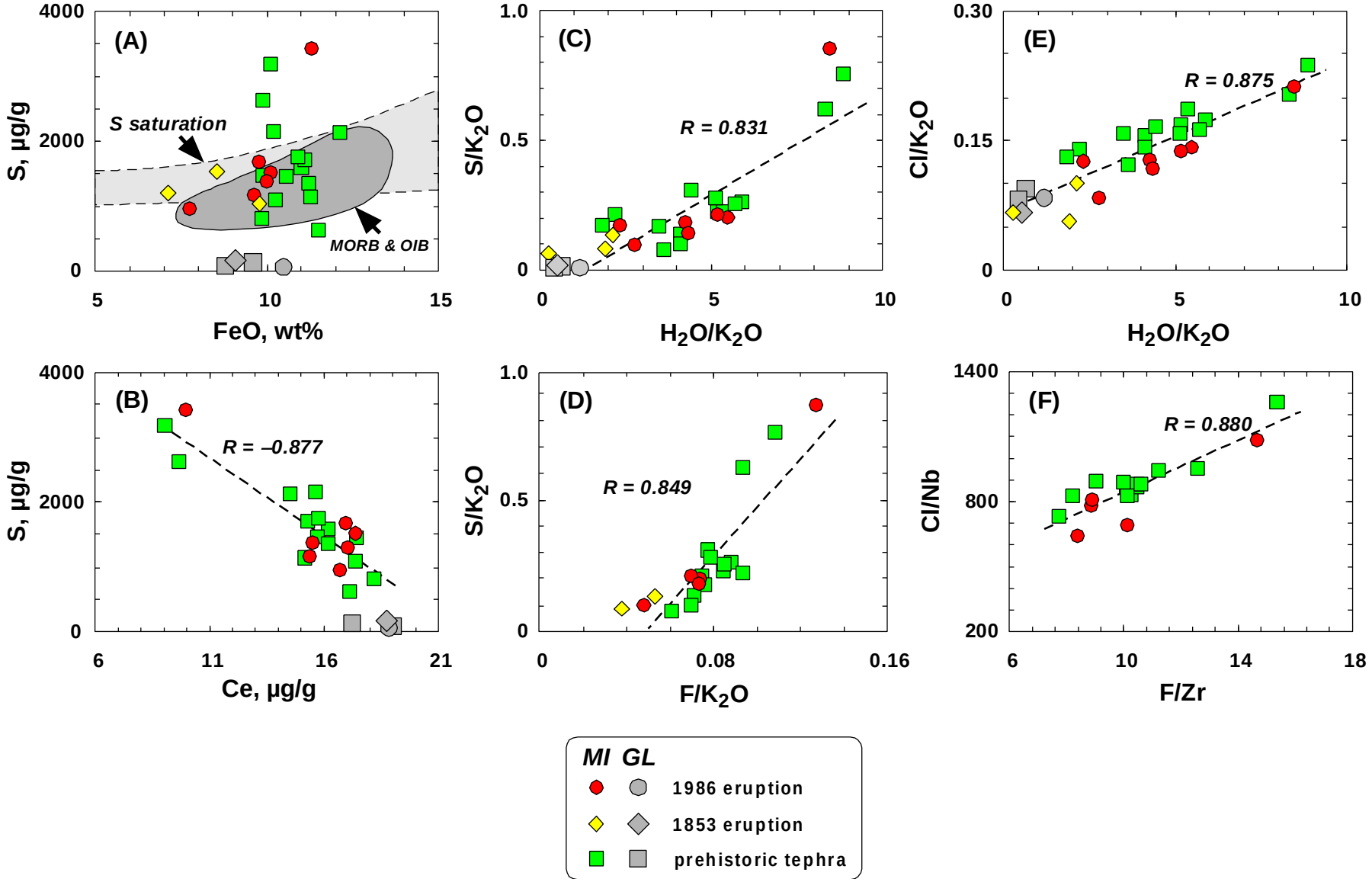

Fig. 5. Gurenko et al.

Figure

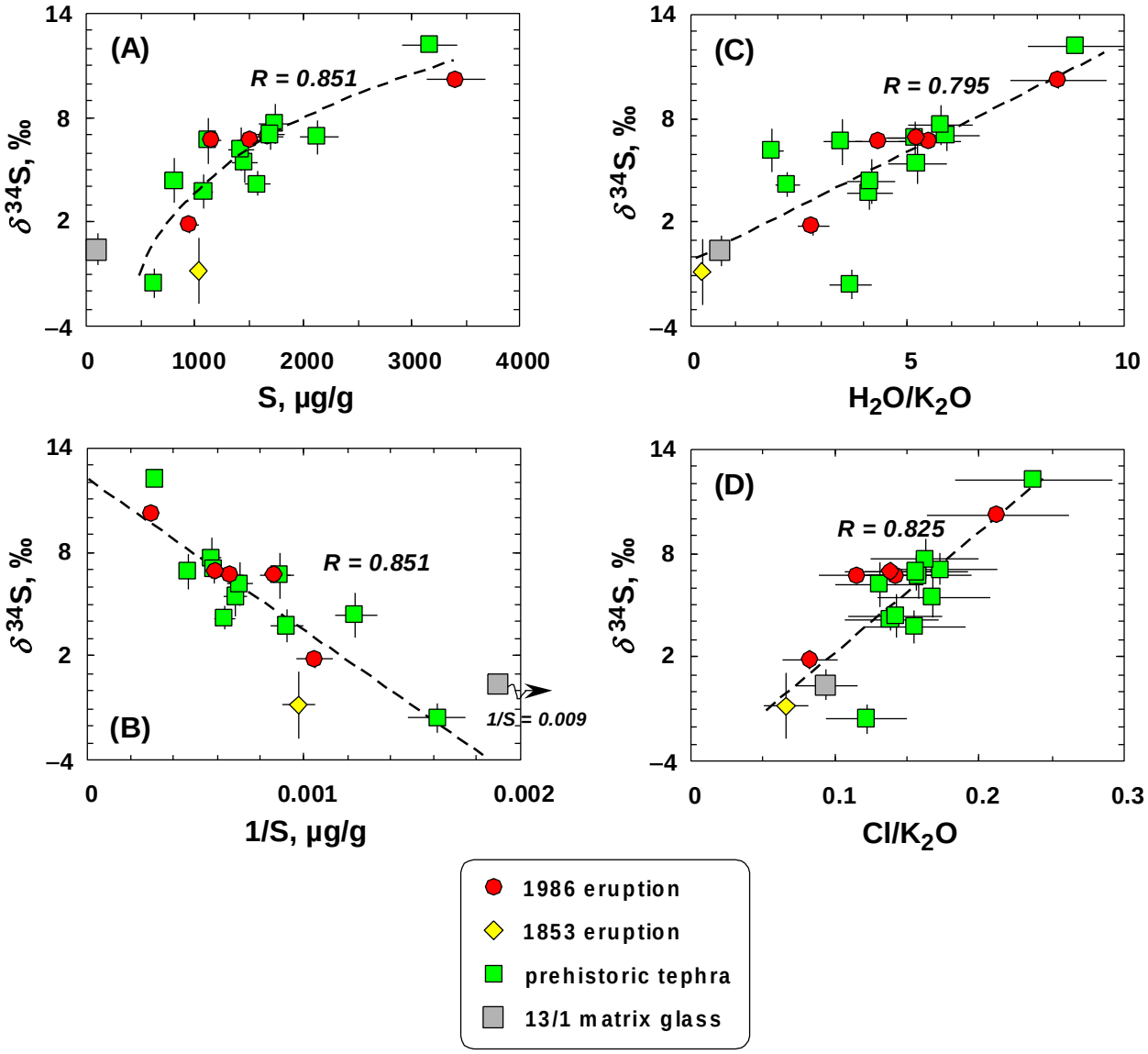

Fig. 6. Gurenko et al.

Figure

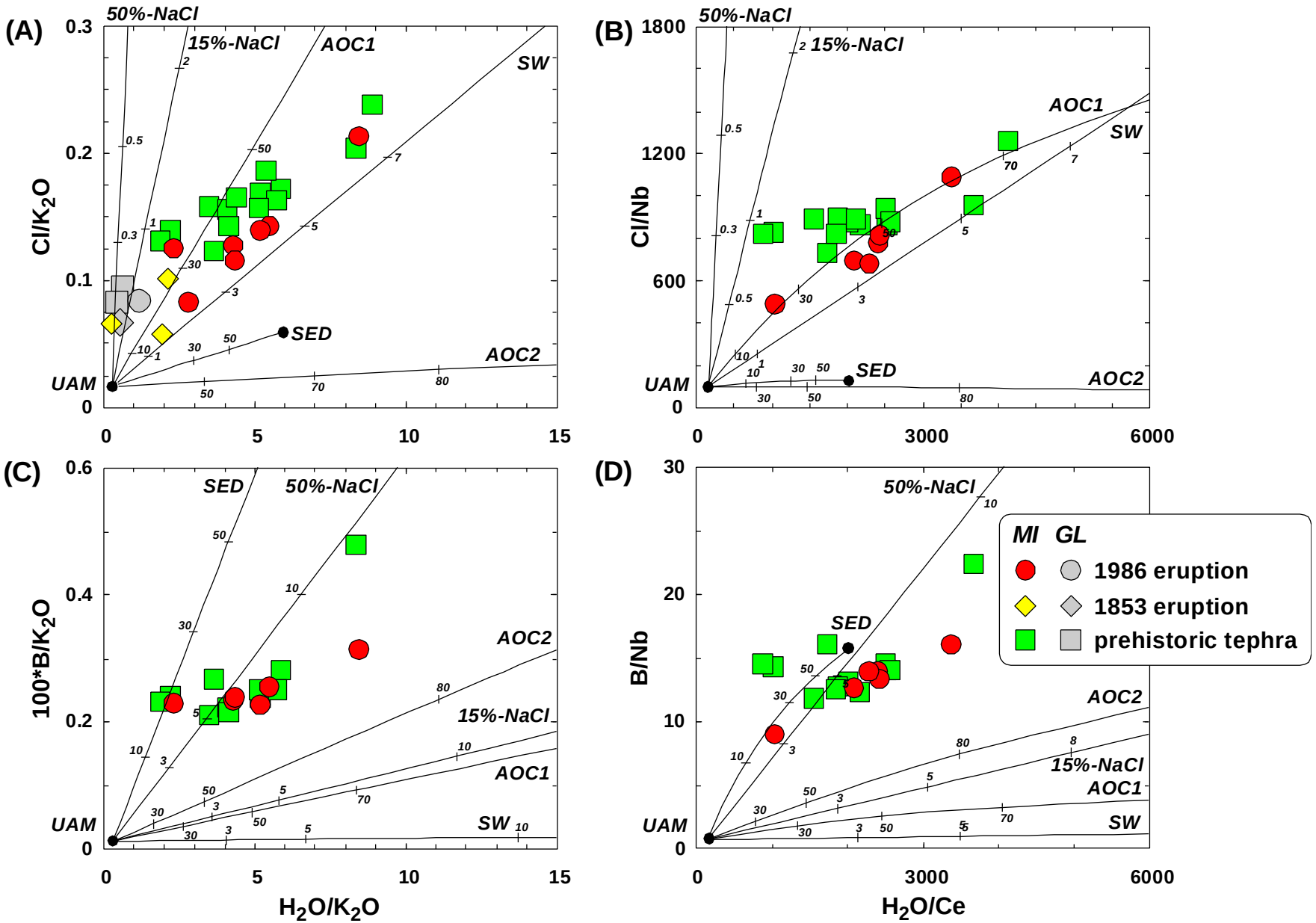

Fig. 7. Gurenko et al.

Figure

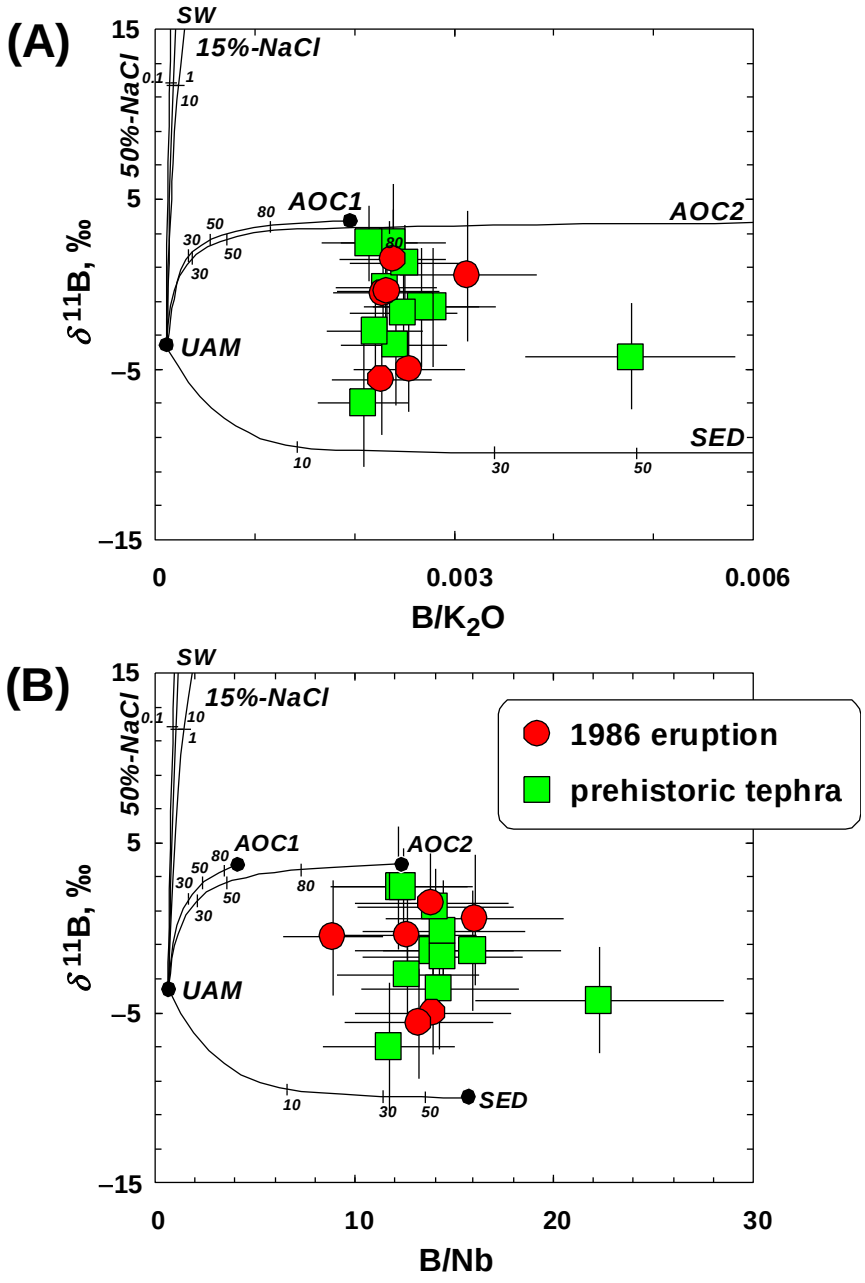

Fig. 8. Gurenko et al.

Figure

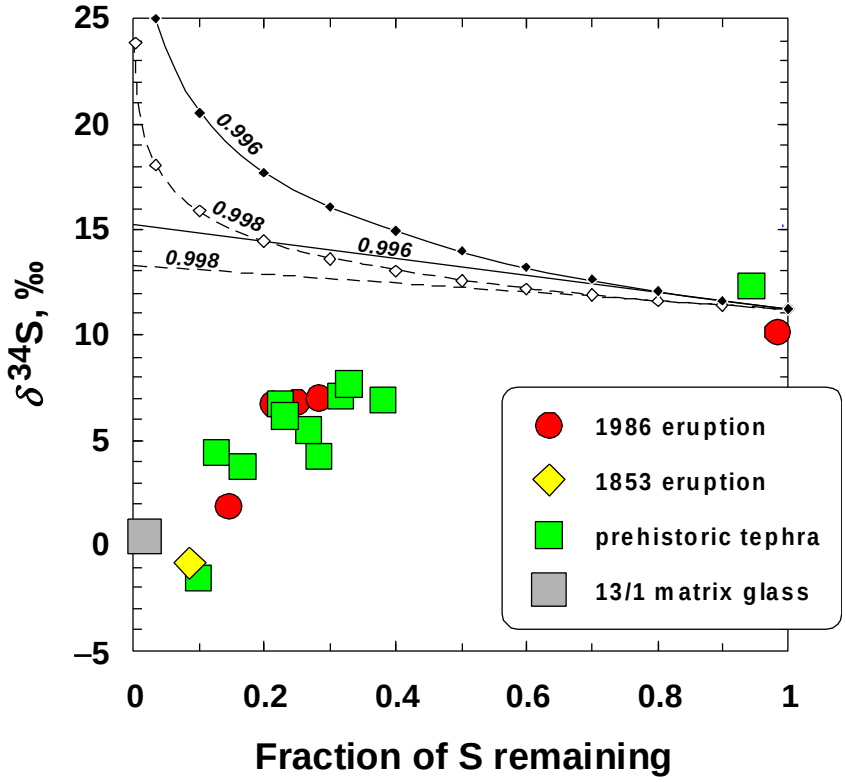

Fig. 9. Gurenko et al.

Figure

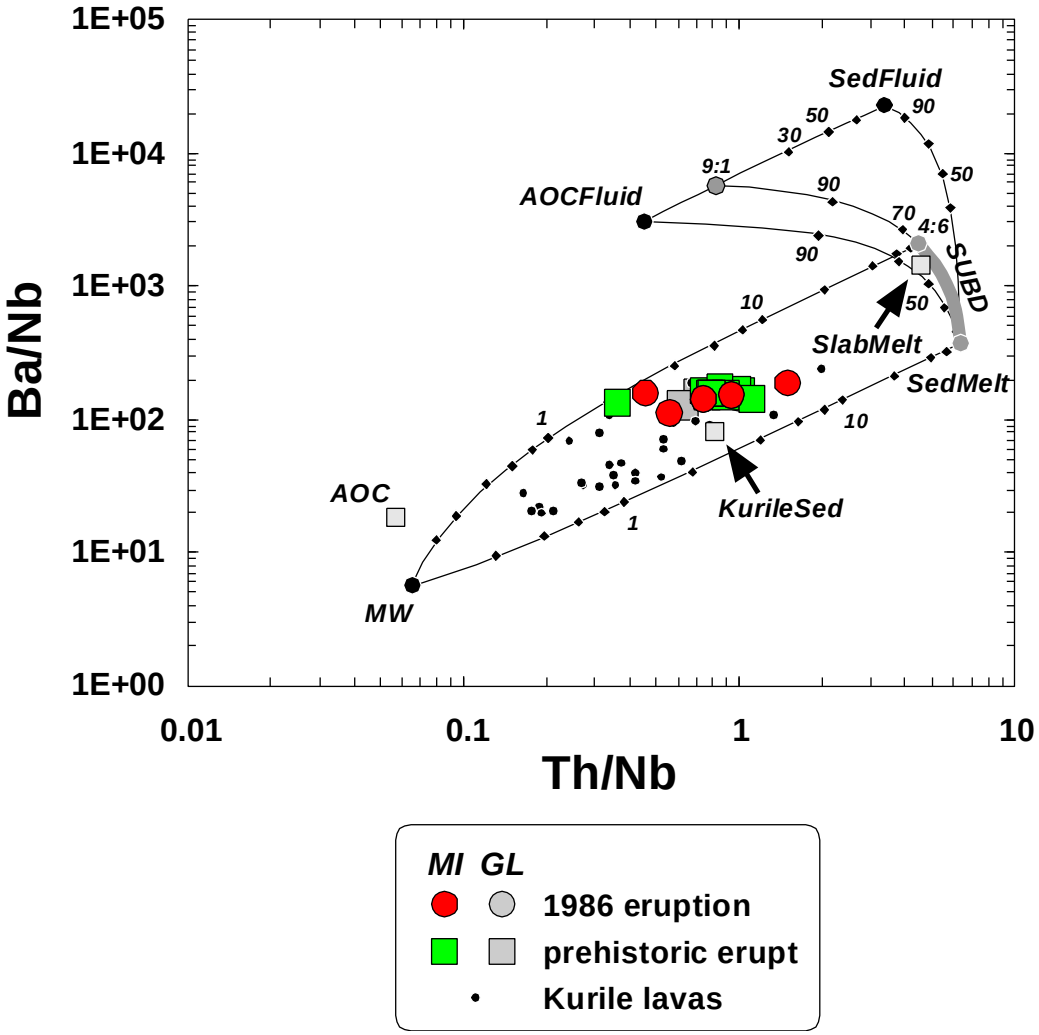

Fig. 10. Gurenko et al.

Figure

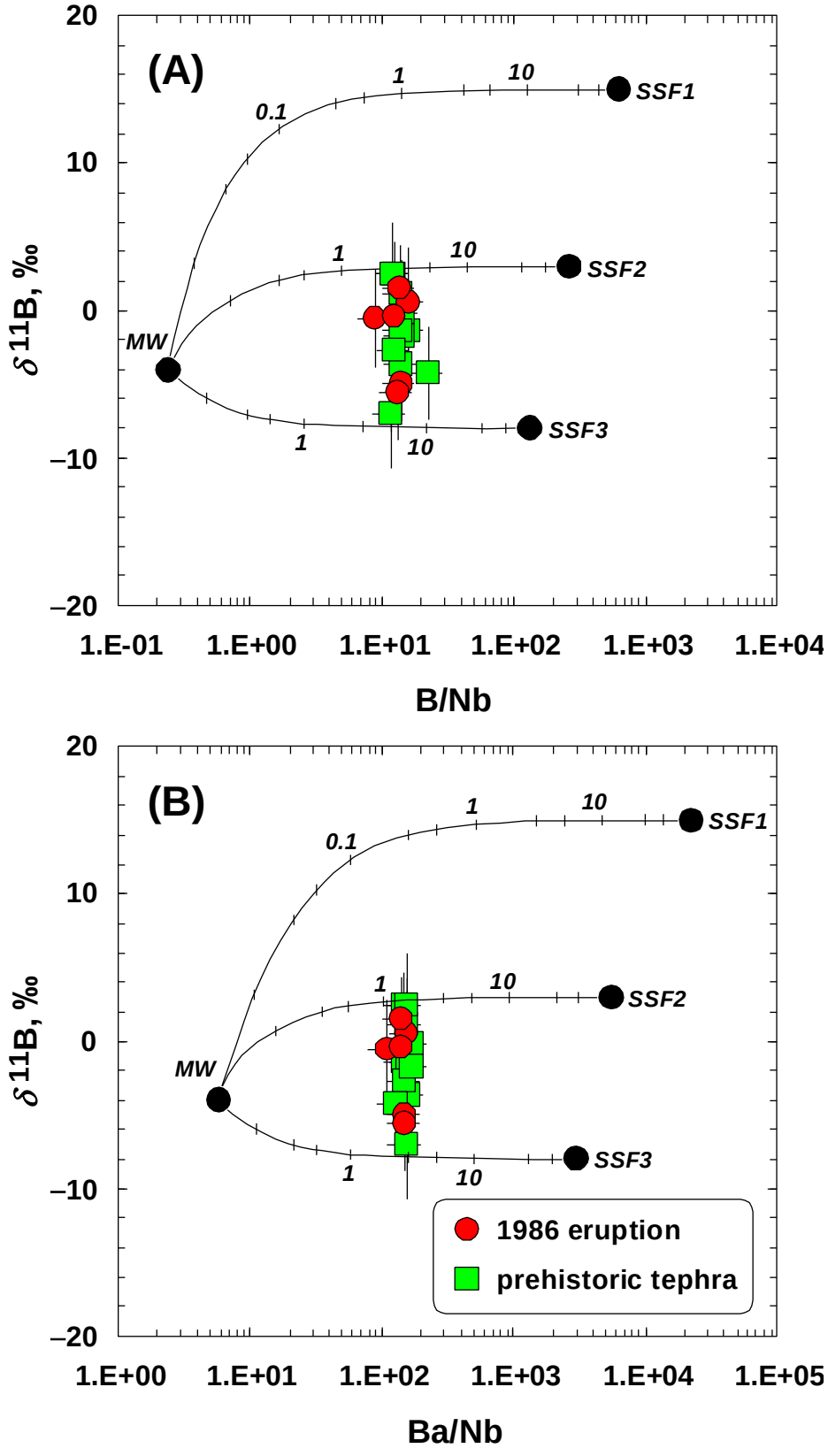

Fig. 11. Gurenko et al.

Background dataset for online publication only

Click here to download Background dataset for online publication only: Chik_d11B-d34S SOM 3.0.pdf